

N,N-Dimethyltryptamine attenuates spreading depolarization and restrains neurodegeneration by sigma-1 receptor activation in the ischemic rat brain

Írisz Szabó^a, Viktória É. Varga^a, Szabolcs Dvorácskó^{b,c}, Attila E. Farkas^d, Tímea Körmöczi^{c,e}, Róbert Berkecz^{c,e}, Szilvia Kecskés^a, Ákos Menyhart^a, Rita Frank^a, Dóra Hantosi^a, Nicholas V. Cozzi^{f,g}, Ede Frecska^h, Csaba Tömböly^b, István A. Krizbai^{d,i}, Ferenc Bari^a, Eszter Farkas^{a,*}

^a Department of Medical Physics and Informatics, Faculty of Medicine and Faculty of Science and Informatics, University of Szeged; Korányi Fásor 9, Szeged, 6720, Hungary

^b Laboratory of Chemical Biology, Institute of Biochemistry, Biological Research Centre, Temesvári Krt 62, Szeged, 6726, Hungary

^c Department of Medical Chemistry, Faculty of Medicine, University of Szeged, Dóm Tér 8, Szeged, 6720, Hungary

^d Neurovascular Unit Research Group, Molecular Neurobiology Research Unit, Institute of Biophysics, Biological Research Centre, Temesvári Krt 62, Szeged, 6726, Hungary

^e Institute of Pharmaceutical Analysis, Faculty of Pharmacy, University of Szeged, Somogyi U 4, Szeged, 6720, Hungary

^f Neuropharmacology Laboratory, University of Wisconsin School of Medicine and Public Health, 1300 University Avenue, Madison, WI 53706, USA

^g Alexander Shulgin Research Institute, 1483 Shulgin Road, Lafayette, CA, 94549, USA

^h Department of Psychiatry, Faculty of Medicine, University of Debrecen, Nagyterdei Krt 94, Debrecen, 4032, Hungary

ⁱ Institute of Life Sciences, UVVG, 94 Bulevardul Revolutiei, Arad, 310025, Romania

ARTICLE INFO

Keywords:

N,N-Dimethyltryptamine
Cerebral ischemia
Sigma-1 receptor
Spreading depolarization
Stroke

ABSTRACT

Dimethyltryptamine (DMT), an endogenous ligand of sigma-1 receptors (Sig-1Rs), acts against systemic hypoxia, but whether DMT may prevent cerebral ischemic injury is unexplored. Here global forebrain ischemia was created in anesthetized rats and aggravated with the induction of spreading depolarizations (SDs) and subsequent short hypoxia before reperfusion. Drugs (DMT, the selective Sig-1R agonist PRE-084, the Sig-1R antagonist NE-100, or the serotonin receptor antagonist asenapine) were administered intravenously alone or in combination while physiological variables and local field potential from the cerebral cortex was recorded. Neuroprotection and the cellular localization of Sig-1R were evaluated with immunocytochemistry. Plasma and brain DMT content was measured by 2D-LC-HRMS/MS. The affinity of drugs for cerebral Sig-1R was evaluated with a radioligand binding assay. Both DMT and PRE-084 mitigated SDs, counteracted with NE-100. Further, DMT attenuated SD when co-administered with asenapine, compared to asenapine alone. DMT reduced the number of apoptotic and ferroptotic cells and supported astrocyte survival. The binding affinity of DMT to Sig-1R matched previously reported values. Sig-1Rs were associated with the perinuclear cytoplasm of neurons, astrocytes and microglia, and with glial processes. According to these data, DMT may be considered as adjuvant pharmacological therapy in the management of acute cerebral ischemia.

1. Introduction

N,N-Dimethyltryptamine (DMT) is a natural indole alkaloid found in

plants (e.g. *Psychotria viridis* and *Diplopterys cabrerana*) and is known for its psychedelic effects when ingested by humans as spiritual medicine or with recreative purposes (e.g. ayahuasca brew) (Luna, 2011). Importantly, DMT has also been identified as an endogenous trace amine in mammalian

* Corresponding author. Department of Medical Physics and Informatics Faculty of Medicine, and Faculty of Science and Informatics University of Szeged, Korányi fásor 9, H-6720, Szeged, Hungary.

E-mail addresses: szabo.irisz@med.u-szeged.hu (Í. Szabó), varga.viktoria.eva.22@gmail.com (V.É. Varga), dvoracsco.szabolcs@brc.hu (S. Dvorácskó), farkas.attilae@brc.mta.hu (A.E. Farkas), kormoczi.timea@med.u-szeged.hu (T. Körmöczi), berkecz.robert@szte.hu (R. Berkecz), szilvikecskes84@gmail.com (S. Kecskés), menyhartakos89@gmail.com (Á. Menyhart), ritafrank993@gmail.com (R. Frank), dora.hantosi@gmail.com (D. Hantosi), cozzi@wisc.edu (N.V. Cozzi), efrecska@hotmail.com (E. Frecska), tomboly.csaba@brc.hu (C. Tömböly), krizbai.istvan@brc.mta.hu (I.A. Krizbai), bari.ferenc@med.u-szeged.hu (F. Bari), farkas.eszter.1@med.u-szeged.hu (E. Farkas).

<https://doi.org/10.1016/j.neuropharm.2021.108612>

Received 20 January 2021; Received in revised form 23 April 2021; Accepted 13 May 2021

Available online 21 May 2021

0028-3908/© 2021 The Author(s).

Published by Elsevier Ltd.

This is an open access article under the CC BY-NC-ND license

(<http://creativecommons.org/licenses/by-nc-nd/4.0/>).

Abbreviations	
2D-LC-HRMS/MS	two-dimensional liquid chromatography coupled to quadrupole-Orbitrap mass spectrometry
2VO	two vessel occlusion
4-HNE	4-hydroxynonenal
5-HTR	serotonin receptor
AADC	aromatic-L-amino acid decarboxylase
aCSF	artificial cerebrospinal fluid
ANOVA	analysis of variance
ATP	adenosine triphosphate
AUC	area under the curve
BSA	bovine serum albumin
CBF	cerebral blood flow
CC3	cleaved caspase 3
DAB	diaminobenzidine
DC	direct current
DG	dentate gyrus
DMSO	dimethyl sulfoxide
DMT	N,N-dimethyltryptamine
EDTA	ethylenediamine tetraacetic acid
ECoG	electrocorticogram
ER	endoplasmic reticulum
GFAP	glial fibrillary acidic protein
HIF-1	hypoxia-inducible factor 1
Iba-1	ionized calcium-binding adapter protein
INMT	indolethylamine N-methyltransferase
i.m.	intramuscular
i.v.	intravenous
LDF	laser-Doppler flowmetry
MABP	mean arterial blood pressure
MAM	mitochondria-associated ER membrane
MAO	monoamine oxidase
NeuN	neuronal nuclear protein
NMDA	N-methyl-D-aspartate
PBS	phosphate buffered saline
PFA	paraformaldehyde
SD	spreading depolarizations
Sig-1R	Sigma-1 receptor
TBS	Tris-buffered saline

tissues (e.g. lung, pineal gland, brain) (Christian et al., 1977; Mandel et al., 1977; Barker et al., 2013) and body fluids (urine, blood plasma and cerebrospinal fluid) (Barker et al., 2012). The actual production of DMT from the amino acid tryptophan in mammalian tissues is supported by the (co-)localization of the enzymes aromatic-L-amino acid decarboxylase (AADC) and indolethylamine-N-methyltransferase (INMT) implicated in DMT biosynthesis (Mavlyutov et al., 2012; Carbonaro and Gatch, 2016; Dean et al., 2019). DMT, however, is rapidly biodegraded by monoamine oxidases (MAO), which may be the reason for the very low endogenous DMT concentration measured (e.g. ng/mL or ng/g tissue). Still, DMT may be encapsulated in neurotransmitter storage vesicles at concentrations regarded to be pharmacologically relevant (Carbonaro and Gatch, 2016).

The physiological and pathophysiological role of endogenous DMT has been the subject of ongoing debate and speculations. Psychedelic and behavioral effects (Jenner et al., 1978), a potential role in psychiatric disorders (Daumann et al., 2010) and altered states of consciousness (Strassman, 2001) have all been attributed to naturally occurring DMT. Besides all of these elusive associations, investigators have recently turned their attention to the prospective general tissue protective (Frecka et al., 2013), and specific neuroprotective potential of the substance (Szabo et al., 2016; Nardai et al., 2020). DMT has been claimed to be produced at increased concentration in the rodent brain when exposed to environmental stress delivered by electrical shock (Barker et al., 1981). More importantly, the DMT content of the rat brain was found elevated after experimental cardiac arrest (Dean et al., 2019). Recently, DMT was shown to protect human primary iPSC-derived cortical neurons against hypoxia, coincident with the reduction of hypoxia-inducible factor-1 (HIF-1) expression and function (Szabo et al., 2016). Further, DMT injected intraperitoneally limited infarct size in a rodent model of focal cerebral ischemia, and facilitated the recovery of motor function following ischemic injury (Nardai et al., 2020). Finally, DMT was suggested to achieve notable anti-inflammatory effects (Szabo et al., 2014), because the serum levels of pro-inflammatory cytokines (TNF- α , IL-1 β , IL-6) were found to be decreased in the presence of DMT in the above rat focal cerebral ischemia model (Nardai et al., 2020).

The pharmacological mechanisms of DMT action have been extensively explored, revealing a complex interaction with numerous signaling pathways including biogenic amine receptors, (Ray, 2010), uptake transporters (Blough et al., 2014), and trace amine-associated receptors (Bunzow et al., 2001). In addition, fundamental evidence has been gathered that DMT acts as an endogenous sigma-1 receptor (Sig-1R) agonist (Fontanilla et al., 2009). Sig-1Rs are intracellular

receptors localized to the segment of the endoplasmic reticulum (ER) membrane, which is apposed to the mitochondrial outer membrane (the mitochondria-associated ER membrane, MAM). Via precise molecular machinery, Sig-1Rs control Ca²⁺ trafficking between the MAM and mitochondria, regulate the expression of specific potassium channels, suppress the generation of reactive oxygen species, and ultimately promote cell survival under stress (Hayashi, 2015; Penke et al., 2018). A wealth of experimental data suggests that Sig-1R activation yields neuroprotection in ischemic stroke. For example, fluvoxamine, a potent antidepressant with high affinity for Sig-1R has been demonstrated to suppress ER stress-related apoptosis, reduce infarct size after focal cerebral ischemia, and alleviate ischemia-linked motor dysfunction in mice (Omi et al., 2014; Sato et al., 2014). These results have been confirmed by increased apoptotic neuronal death in Sig-1R knockout mice exposed to global forebrain ischemia, and the suppression of ischemia-induced apoptosis in wild-type mice by the administration of PRE-084, a selective Sig-1R agonist pharmacoon (Zhao et al., 2019). Coincidentally, a significant upregulation of Sig-1R has been linked to the ischemic penumbra (Zhang et al., 2017). Collectively, these data are highly suggestive that Sig-1R activation may be exploited for the purpose of ischemic neuroprotection.

Here we set out to explore whether DMT administration achieves neuroprotection via Sig-1R activation in the acute phase of experimental, transient, cerebral forebrain ischemia, which we aggravated by the recurrent induction of spreading depolarizations (SD) (Somjen, 2001) and a subsequent transient hypoxic episode. We have chosen to induce SDs and an episode of anoxia superimposed on global cerebral ischemia to increase the metabolic stress to a level which may cause acute neurodegeneration and is relevant to observe DMT action. Incidentally, SD initiates the fission of the ER (the intracellular host of Sig-1Rs), which may serve as a target of neuroprotection (Kurcharz and Lauritzen, 2018). The physiological impact of administered DMT was evaluated by the assessment of cerebral blood flow (CBF) variations and the characteristic features of SD, a neurophysiological phenomenon that had been recognized to accelerate the conversion of the ischemic penumbra to the infarcted region (Hartings et al., 2017). Furthermore, SD is a relevant target of investigation in the context of neuroprotection, because SD inhibition has been repeatedly proposed as an effective approach for tissue salvage in brain injury (Carlson et al., 2018, 2020; Klass et al., 2018; Varga et al., 2020). As a final point in our experiments, DMT-related neuroprotection was evaluated with comprehensive histological examination.

To confirm the role of Sig-1Rs in the DMT-linked effects, we measured the binding affinity of DMT to Sig-1Rs in rat brain tissue and we evaluated the response to DMT in the presence of the selective Sig-1R agonist PRE-084 or the Sig-1R antagonist NE-100. To discriminate the potential contribution of serotonin receptors to DMT-related effects, asenapine, an antagonist of a wide range of serotonin receptors (Shadid et al., 2009), was applied alone, or in combination with DMT. Next, to confirm that DMT infused over the experimental protocol accumulated in the blood and brain to a pharmacologically relevant concentration, we determined the DMT content in these tissues with an analytical chemical method (Körmöczki et al., 2020). Finally, we confirmed the co-localization of Sig-1Rs with neurons, astrocytes and microglia cells, as potential cellular targets of DMT treatment.

2. Materials and methods

The ethical approach conformed to previously reported guidelines (Szabó et al., 2019; M. Tóth et al., 2020; Varga et al., 2020), and the experiments are reported in compliance with the ARRIVE guidelines (Kilkenny et al., 2010). The experimental procedures were approved by the National Food Chain Safety and Animal Health Directorate of Csongrád County, Hungary. The procedures were performed according to the guidelines of the Scientific Committee of Animal Experimentation of the Hungarian Academy of Sciences (updated Law and Regulations on Animal Protection: 40/2013. (II. 14.) Gov. of Hungary), following the EU Directive 2010/63/EU on the protection.

The animals were housed according to standard conditions reported earlier (Szabó et al., 2019; M. Tóth et al., 2020; Varga et al., 2020). Young adult, male Sprague-Dawley rats (Charles River Laboratories, 340 ± 37 g, n = 69) were used in this study. Standard rodent chow and tap water were supplied *ad libitum*. The animals were housed under constant temperature, humidity, and lighting conditions (23°C, 12:12 h light/dark cycle, lights on at 7 a.m.).

The estimation of sample size adhered to previously applied principles (Szabó et al., 2019; Varga et al., 2020). The designed rate of the seven groups of the *in vivo* experiment (untreated and treated) was 1. The necessary number of animals in each group was at least 6 to support 80% power ($\beta = 20\%$ risk of second species), which was calculated based on the standard deviation of electrophysiological and hemodynamic parameters in earlier studies and the presumed differences between the means of groups. The calculations and statistical analyses were conducted in SPSS version 20 (Vanderbilt University, U.S.A.) and were also run in GPower 3.1 (Heinrich Heine University of Düsseldorf, Germany).

2.1. Surgical procedures

The preparation has followed previously established guidelines (Szabó et al., 2019; Varga et al., 2020). On the day of the experiments, animals were anesthetized with 1.5–2% isoflurane in N₂O:O₂ (3:2), and were allowed to breathe spontaneously through a head cone during surgical interventions (n = 56). Body temperature was kept at 37.2 °C by a feedback controlled heating pad (Harvard Apparatus, Holliston, MA, U.S.A.). In order to avoid the production of airway mucus, atropine was administered (0.1%, 0.05 mL; i.m.) shortly before surgical procedures. The left femoral artery was cannulated for blood sampling and the continuous monitoring of mean arterial blood pressure and heart rate (MABP, Mikro-Tip BP Foundation System, ADInstruments, Australia). The adjacent femoral vein was also cannulated for the administration of drugs.

Actual surgical procedures have also replicated previously established methods (Szabó et al., 2019; Varga et al., 2020). For the later initiation of incomplete global forebrain ischemia, a midline incision was made in the neck and both common carotid arteries were carefully separated from the vagal nerves. Lidocaine (1%) was administered topically before opening the skin and each tissue layer underneath. A surgical thread used as occluder was looped around each artery for the

later occlusion. All rats were placed prone in a stereotaxic apparatus. The skin above the skull and the temporal muscle were retracted from the underlying left parietal and temporal bones. Two cranial windows (~3 × 3 mm) 1 mm apart were prepared over the right parietal cortex (3 mm from bregma and 5 mm lateral from the sagittal suture) (Fig. 1). A high-precision electrical drill (ProLab Basic, Bien Air 810, Switzerland) was used to thin the bone under saline cooling, and the remaining soft bone layer was gently peeled away to reveal the dura surface. The dura was then carefully opened in each craniotomy. The rostral window was later used for data acquisition (i.e. electrophysiology and CBF measurement) while the caudal window served SD elicitation (Fig. 1). The cranial windows were constantly kept moist by artificial cerebrospinal fluid (aCSF; mM concentrations: 126.6 NaCl, 3 KCl, 1.5 CaCl₂, 1.2 MgCl₂, 24.5 NaHCO₃, 6.7 urea, 3.7 glucose bubbled with 95% O₂ and 5% CO₂ to achieve a constant pH of 7.4).

2.2. Recording of electrophysiological variables

Electrophysiological data were acquired as reported earlier (Szabó et al., 2019; Varga et al., 2020). For the acquisition of the electrocorticogram (ECoG) and slow cortical or direct current (DC) potential, a saline-filled (120 mM NaCl) glass capillary microelectrode (20 µm outer tip diameter) was inserted 700 µm deep into the right somatosensory cortex. An Ag/AgCl reference electrode was implanted under the skin of the animal's neck. The electrophysiological signals were recorded via a high input impedance pre-amplifier (NL102GH, NeuroLog System, Digitimer Ltd., United Kingdom), connected to a differential amplifier (NL106, NeuroLog System, Digitimer Ltd., United Kingdom) with associated filter (ECoG filtered in wideband scale: 0.5–35 Hz, DC filtered in DC mode; <0.5 Hz) and conditioner systems (NL125, NL144, NL530, NeuroLog System, Digitimer Ltd., United Kingdom). Line frequency noise (50 Hz) was removed by a high-quality noise eliminator (HumBug, Quest Scientific Instruments Inc., Canada). The electrical signals along with MABP were digitalized at a sampling frequency of 2 kHz by a PowerLab data acquisition device (ADInstruments, Australia) controlled through a dedicated software written in LabChart 8 (ADInstruments, Australia).

2.3. Monitoring of local cerebral blood flow

CBF measurements were conducted as reported earlier (Szabó et al., 2019). Laser-Doppler flowmetry (LDF) was used to record changes in local CBF with ischemia/reperfusion, and associated with SD events. A laser-Doppler needle probe (Probe 403 connected to PeriFlux 5000; Perimed AB, Sweden) was positioned above the parietal cortex. The ideal position of the LDF probe was identified prior to the actual experimental protocol: the probe was positioned over the region where the baseline perfusion varied closely around 300 perfusion units (PFU), as near as possible to the tip of the glass microcapillary, and avoiding visible pial blood vessels. The LDF signal was digitalized and acquired, together with the DC potential and ECoG, essentially as described above.

2.4. Pharmacological treatment

All drugs were dissolved in physiological saline, administered at a dose of 1 mg/kg/h (Maurice et al., 1995; Ghanbari et al., 2009; Sato et al., 2014; Nardai et al., 2020), and infused through the left femoral vein continuously throughout the experimental protocol (Fig. 1). Although DMT has poor solubility in aqueous media, intensive vortexing at 37 °C resulted in a transparent solution at the low concentration used. The concentration of the DMT solution was 0.18 mg/mL (0.956 mM). The following treatments were applied: DMT (Lipomed AG, Switzerland) alone (n = 7), the highly selective Sig-1R agonist PRE-084 (Sigma-Aldrich, U.S.A.) alone (n = 8), the selective Sig-1R antagonist NE-100 (Sigma-Aldrich, U.S.A.) alone (n = 6) or in combination with DMT (n = 6), and the non-subtype specific serotonin receptor (5-HT₂)

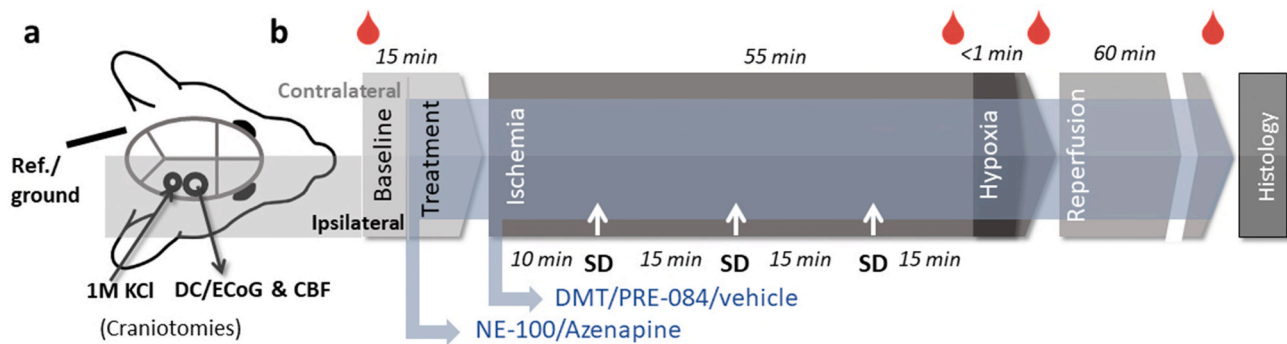


Fig. 1. Graphical illustration of the experimental protocol. **a**, In the preparation, black circles indicate the position of the two open cranial windows (3 mm caudal from bregma and 5 mm lateral from the sagittal suture), created for the recording of the electrocorticogram (ECoG), direct current (DC) potential and cerebral blood flow (CBF) with laser-Doppler flowmetry (rostral window) and the experimental elicitation of spreading depolarizations (SD) with KCl (caudal window). **b**, The schematic drawing illustrates the subsequent phases of the experimental protocol. After the initiation of global forebrain ischemia, the i.v. infusion of either of the Sig-1R agonists (DMT or PRE-084) or their vehicle was initiated and maintained until the termination of the experiment. When the Sig-1R or the serotonin receptor (5-HT₂) antagonists NE-100 or asenapine were applied, their i.v. infusion was initiated before ischemia onset. Subsequently, SDs were triggered at the ipsilateral cerebral cortex, then O₂ was partially and briefly withdrawn from the anesthetic gas mixture to aggravate ischemia further by transient hypoxia. After an hour of reperfusion, the brains were removed under deep anesthesia for histological examination. Arterial blood samples were collected repeatedly (●) for blood gas analysis and the measurement of blood plasma DMT content.

antagonist asenapine (Sigma-Aldrich, U.S.A.) alone (n = 6) or in combination with DMT (n = 6). Vehicle (i.e. physiological saline) served as control for the treatments (n = 7). NE-100 and DMT or asenapine and DMT were used in combination to test the receptor-specificity of DMT.

2.5. Experimental protocol

The experimental protocol was initiated 30–60 min after completion of the preparation. After a baseline period (5 min), cerebral ischemia was induced by the occlusion of both common carotid arteries (two vessel occlusion: 2VO). Successful 2VO was confirmed by a sharp drop of CBF below 50% of baseline, as reported earlier (Menyhárt et al., 2017; Szabó et al., 2019). Ischemia induction was not followed by spontaneous SD occurrence, probably because the hypoperfusion threshold to trigger SD (Menyhárt et al., 2017) was not reached. The administration of DMT, PRE-084, or vehicle was initiated through the femoral vein immediately after completion of the ischemia induction, with the aid of a micro-injector syringe pump (CMA/100 Micro Injection Pump, Carnegie Medicin, Sweden). Due to the dead volume in the tubing, it could have taken a few minutes before the DMT solution actually reached the brain. Residual CBF during ischemia varied around 40% (see: Results – Physiological variables), which was considered sufficient for drug delivery. In the case of DMT co-application with NE-100 or asenapine, the infusion of NE-100 or asenapine began 10 min before ischemia induction to act on receptors before DMT application. The intravenous (i.v.) infusion of the drugs was continuous and maintained until the end of the experiment.

As further metabolic challenge superimposed on ischemia, three SD events were triggered at an inter-SD interval of at least 15 min with a 1 M KCl-soaked cotton ball placed on the cortex in the caudal craniotomy (Farkas et al., 2011), starting 10 min after 2VO onset (Fig. 1). The cotton ball was removed and the craniotomy rinsed with aCSF after each SD event. After the three SDs had subsided, the ischemic insult was further aggravated by an episode of transient hypoxia (maximum of 1 min) achieved by the controlled withdrawal of O₂ from the anesthetic gas mixture. The duration of hypoxia had been determined in pilot experiments. Longer episodes of hypoxia caused the failure of cardiac function, therefore we adjusted hypoxia duration according to the tolerance of each animal: hypoxia was maintained in the presented experimental protocol as long as arterial pressure (monitored continuously live) was stable enough for prospective recovery from the insult. The hypoxic

episode was followed by reoxygenation and the prompt release of the common carotid arteries to afford cerebral reperfusion for another hour.

2.6. Immunocytochemistry

Immunolabeling followed procedures that are in routine use in our lab (M. Tóth et al., 2020; Varga et al., 2020). For all staining protocols, antibody specificity was confirmed by performing the staining in the absence of the primary antibody in the solution prepared for the primary incubation step. Naive (n = 3), and vehicle- or DMT-treated rats exposed to the full experimental protocol (i.e. 2 h after ischemia induction and 1 h after reperfusion induction; n = 4/4) were transcardially perfused with ice-cold physiological saline followed by 4% paraformaldehyde (PFA) under deep anesthesia (5%, i.p., 500 mg/kg). The brains were removed, stored in 4% PFA at 4 °C overnight, and cryoprotected in 30% sucrose in phosphate buffered saline (PBS). Coronal, 20 μm thick fore-brain sections were cut with a freezing microtome (Leica CM, 1860 UV, Leica, Germany).

Apoptotic cell death was characterized with permanent immunocytochemical staining of cleaved caspase-3 (CC3), ferroptotic injury by 4-hydroxynonenal (4-HNE), whereas neuronal loss was identified with the neuron marker neuronal nuclear protein (NeuN), and astrocyte damage with the astrocyte marker glial fibrillary acidic protein (GFAP) on selected coronal slices (bregma +1, –3 and –6 mm, Paxinos and Watson atlas coordinates; three slices per plane). Microglial activation was detected with ionized calcium-binding adapter protein (Iba-1) immunohistochemistry. In all cases, endogenous peroxidases were blocked with 5% H₂O₂, nonspecific protein-binding sites were blocked with 5% normal goat serum (Merck, Kenilworth, U.S.A.), and slices were permeabilized with 0.5% Triton X-100 (Merck, Kenilworth, U.S.A.) in Tris-buffered saline (TBS). Slices were incubated with rabbit anti-CC3 (Abcam, ab13847, 1:300), mouse anti-4-HNE (Abcam, ab48506, 1:100), rabbit anti-NeuN (Abcam, ab177487, 1:300), mouse anti-GFAP (Abcam, ab4648, 1:1000) or rabbit anti Iba-1 (Wako, #019–19741, 1:3000) overnight at 4 °C. The subsequent steps of incubation included an enhancer reagent for 1 h at room temperature, and horseradish-peroxidase-linked secondary antibody for 3 h at room temperature, both being components of the Polink-2 Plus HRP Detection Kit (for rabbit or mouse primary antibody with diaminobenzidine (DAB) chromogen, D39–18 for rabbit and D37–18 for mouse, GBI Labs, U.S.A.). The staining was visualized with DAB. The slices were mounted on microscopic slides with Eukit® (Merck, U.S.A.) and photomicrographs were obtained with a Nikon-DS Fi3 camera attached to a Leica DM 2000 Led

light microscope (Leica Microsystems GmbH, Germany).

Finally, in order to identify the cellular and subcellular localization of Sig-1Rs, the receptors were co-labeled with NeuN (neuronal marker), GFAP (astrocyte marker) and Iba-1 (microglia marker) in slices from a naïve animal. Antigens were retrieved with 10-min-long boiling in 6 M urea in Tris-HCl buffer (pH 9.5; 80 °C, shaking at 300 rpm) (Hayashi et al., 2011). All slices were permeabilized with 0.2% Triton X-100 in PBS for 30 min. Non-specific protein-binding sites were blocked with 3% bovine serum albumin (BSA) for 1 h at room temperature. Slices were incubated with primary antibodies overnight at 4 °C (anti-Sig-1R: rabbit, Abcam, ab53852, 1:500; anti-NeuN: mouse, Millipore, MAB377, 1:250; anti-GFAP: mouse, Sigma, G3893, 1:500; anti-Iba-1: mouse, Wako, #016–26721, 1:200 in 3% BSA in PBS). Secondary antibodies were applied for 1 h at room temperature (anti-rabbit STAR RED; goat, Abberior, 1:500 and anti-mouse STAR 580, goat, Abberior, 1:500 for NeuN and GFAP-labelling; anti-rabbit Alexa-488, goat, Thermo Fisher Scientific, #A11034, 1:500, anti-mouse Alexa-647, donkey, Thermo Fisher Scientific, #A32787, 1:500 for Iba-1 labelling) in 1% BSA in PBS. Slices were mounted with Mount Solid antifade© (Abberior, Germany). Representative epifluorescent (20x) and confocal (100x) images were taken of the somatosensory cortex with a Zeiss Axio Observer Z1 inverted microscope (Carl Zeiss GmbH, Germany) equipped with a laser confocal imaging capable Stedycyon (Abberior Instruments, Germany), and pieced together, re-coloured and processed in ImageJ (National Institutes of Health, Bethesda, Maryland, USA) (Schneider et al., 2012).

2.7. *In vitro* radioligand binding assay

PRE-084 (Sig1-R agonist), asenapine (5-HTR antagonist), fluvoxamine (Sig-1R agonist), (+)-pentazocine (Sig-1R agonist), haloperidol (Sig-1R antagonist) and buffer components (TRIS-HCl) were purchased from Sigma-Aldrich Kft. (Budapest, Hungary). The radioligand [³H]-(+)-pentazocine (specific activity 1.98 TBq/mmol) was prepared in the Laboratory of Chemical Biology (BRC, Hungary). Tritium labeling was carried out in a self-designed vacuum manifold (Dvorácskó et al., 2019) and radioactivity was measured with a Packard Tri-Carb 2100 TR liquid scintillation analyzer using Insta Gel scintillation cocktail of PerkinElmer. Drugs were dissolved at 100 mM (DMT) or 1 mM (PRE-084, (+)-pentazocine, asenapine, fluvoxamine) in dimethyl sulfoxide (DMSO) and were stored at –20 °C, and then diluted in the binding buffer.

Preparation of rat brain tissue membrane homogenates was performed according to a previous method (Narita et al., 1996; Ishima et al., 2014), with a slight modification. Male Sprague–Dawley rats (n = 10, 250 g) were decapitated in deep anesthesia, and their brains were removed rapidly. The brains without cerebellum were homogenized in 20 vol of ice-cold 50 mM Tris-HCl (pH 8.0 at 25 °C), using a Braun Teflon-glass homogenizer at the highest speed for 30 s. The homogenate was centrifuged at 48.000 g for 10 min at 4 °C. The resulting pellet was resuspended in 50 mM Tris-HCl buffer (pH 8.0) and recentrifuged. This procedure was repeated twice. The final pellet was suspended in 20 vol of 50 mM Tris-HCl (pH 8.0) and stored in aliquots at –80 °C. The protein content of the samples was measured by the Bradford method (Bradford, 1976) and samples were diluted to obtain the appropriate amount for the assay.

Binding assays for the Sig-1R followed previously established methods with slight modification (Ishima et al., 2014). Samples were incubated at 27 °C for 120 min in a 50 mM Tris-HCl binding buffer (pH 8.0) in plastic tubes in a total assay volume of 1 mL that contained 0.5 mg/mL of membrane protein. Competition binding experiments were carried out by incubating rat brain membranes with 3.6 nM of [³H]-(+)-pentazocine (K_d = 13.1 nM) in the presence of increasing concentrations (10^{–11}–10^{–3} M) of various competing unlabeled ligands. Non-specific binding was determined in the presence of 10 μM haloperidol. The incubation was terminated by diluting the samples with ice-cold wash buffer (50 mM of Tris-HCl, pH 8.0), followed by repeated

washing and rapid filtration through Whatman GF/B glass fiber filters (Whatman Ltd., Maidstone, England) presoaked with 0.1% polyethyleneimine. Filtration was performed with a 24-well Brandel Cell Harvester (Gaithersburg, MD, U.S.A.). Filters were air-dried and immersed into Ultima Gold MV scintillation cocktail, and then radioactivity was measured with a TRI-CARB 2100 TR liquid scintillation analyzer (Packard, PerkinElmer, Waltham, MA, U.S.A.).

2.8. Measurement of exogenous DMT in rat tissue

Because the enzymatic degradation of DMT is rapid, we set out to confirm that DMT supplied to the animals was present at detectable levels and sufficient concentration in the blood plasma and brain to potentially achieve neuroprotection. Blood samples were collected through the femoral artery at baseline (i.e. prior to ischemia onset), under ischemia, after hypoxia, and under reperfusion (n = 4/4, vehicle/DMT). Full blood was centrifuged promptly in EDTA coated Eppendorf tubes (5000 G, 5 min, 4 °C, Heraeus Fresco 17 Microcentrifuge, Thermo Scientific, U.S.A.), and supernatant plasma (0.2 mL) was separated into another Eppendorf vial. To collect brain tissue samples, the animals (n = 4/4, vehicle/DMT) were transcardially perfused with ice-cold physiological saline under deep anesthesia (5%, i.p., 500 mg/kg) at the end of the experimental protocol to wash out any blood from the brain. The full brains were quickly removed, snap-frozen in liquid nitrogen, and stored at –70 °C until further processing. The DMT content of blood plasma and brain tissue was measured by using heart-cutting two-dimensional liquid chromatography coupled to quadrupole-Orbitrap mass spectrometry (2D-LC-HRMS/MS), which is presented in detail in a previous study (Körmöczsi et al., 2020).

2.9. Data analysis

Data analysis was conducted according to established principles (Szabó et al., 2019; M. Tóth et al., 2020; Varga et al., 2020). Physiological variables (i.e. DC potential and MABP) were simultaneously acquired, displayed live, and stored using a personal computer equipped with the software LabChart 8 (ADInstruments, Australia). Data analysis was assisted by the inbuilt instructions of the software AcqKnowledge 4.2 for MP 150 (Biopac Systems, Inc., Goleta, U.S.A.). Blinding data analysis was intended by assigning codes to files and recordings, which do not reveal the experimental condition (i.e., date of the experiment). The experimental data were not processed in cases the animals died during SD elicitation or due to the hypoxic episode (n = 6, random distribution over pharmacological treatments).

Raw LDF recordings were downsampled to 1 Hz and expressed relative to baseline by using the average CBF value of the first 5 min (100%) and the recorded biological zero obtained after the termination of the experiments (0%) as reference points. Raw DC recordings were also downsampled to 1 Hz.

For SD events, peak amplitude, duration at half amplitude, the rate of depolarization and repolarization, and area under the curve (AUC) were measured on the DC potential trace of all three SDs. The SDs elicited were associated with a prominent hyperemia, rather than spreading ischemia, because CBF during ischemia was approximately around the upper limit typical of the ischemic penumbra (i.e. 40 % relative to baseline). The CBF response to SD tends to be hyperemic under such flow conditions, which we have shown earlier (Bere et al., 2014). For SD-associated hyperemia, only the second and third SDs were considered, due to the substantially different CBF response to the first SD. Peak amplitude, duration at half amplitude, the rate of depolarization and repolarization, and AUC were measured.

The CC3-labeled and 4-HNE slides were evaluated by manual cell counting with the CellCounter plugin of ImageJ (National Institutes of Health, Bethesda, Maryland, USA) by two observers blind to the experimental design. Cell count was expressed for a unit surface of 1 mm². The intensity of the 4-HNE labeling was estimated for the

perinuclear cytoplasm of CA1 pyramidal cells and granule cells of the dentate gyrus. The cellular cytoplasm of individual labeled cells was delineated manually. The density of the labeling was evaluated with respect to background by the NIS Elements Advanced Research Software (Version 5.20, Nikon) (Nikon Instruments, Tokyo, Japan). Neuronal and astrocytic loss was characterized by the estimation of NeuN- or GFAP-positive immunolabeling, respectively, in all observed brain regions. After masking binary images in ImageJ, the relative surface covered by immunopositive cells was expressed. The Iba-1 labelling was evaluated with a ramification index as previously described (Tóth et al., 2020). Briefly, a lower ramification index value represents a more activated microglial status.

Data and statistical analysis followed previously accepted guidelines (Szabó et al., 2019; Varga et al., 2020). Data are given as mean ± standard deviation (stdev). The results were statistically analyzed with the software SPSS (IBM SPSS Statistics for Windows, Version 23.0, IBM Corp.). A Grubbs test was applied to identify potential outliers (n = 4, random distribution over pharmacological treatments). The normal distribution of data sets was evaluated with a Shapiro–Wilk test. In case the data showed normal distribution, an independent samples *t*-test, a one-way analysis of variance (ANOVA) or a two-way ANOVA model was used, dependent on the type of data set. A Fisher post hoc test was used for group comparisons, whenever applicable. In case of nonnormal distribution, a Kruskal–Wallis H test was applied, followed by a Mann–Whitney *U* test for group comparisons. Levels of significance were defined as *p* < 0.05* and *p* < 0.01**. All relevant statistical methods are given in each figure legend.

The results of the competition binding studies are reported as earlier (Ishima et al., 2014). Data are provided as means ± standard error of the mean (S.E.M.) of at least three independent experiments, each performed in duplicate. In competition binding studies, the inhibitory constants (*K_i*) were calculated from the inflection points of the displacement curves using nonlinear least-square curve fitting and the Cheng–Prusoff equation, $K_i = EC_{50}/(1 + [ligand]/K_d)$. *K_i* values of DMT in the absence or presence of 10 μM asenapine were compared by unpaired *t*-test with two-tailed *P* value. One sample *t*-test with a hypothetical value of 100% was applied when specific binding values were compared to total specific binding (100%) in receptor binding assays. Significance was accepted at *P* < 0.05 level. All data and curves were analyzed by GraphPad Prism 5.0 (San Diego, CA, U.S.A.).

3. Results

3.1. Physiological variables

Blood gases varied in the physiological range throughout the experimental protocol, yet these physiological variables significantly shifted over the reperfusion period with respect to baseline and ischemia/hypoxia. In particular, by the end of the reperfusion period, blood pH showed a decreasing tendency (*pH* 7.27 ± 0.17 vs. 7.31 ± 0.11 and 7.30 ± 0.12, reperfusion vs. baseline and ischemia/hypoxia; *F* = 2.525, *p* < 0.085), *pCO*₂ noticeably increased (42.3 ± 13.6 vs. 33.2 ± 7.6 and 34.3 ± 10.5 mmHg, reperfusion vs. baseline and ischemia/hypoxia; *F* = 9.102, *p* < 0.0003**) and *pO*₂ decreased (99.6 ± 24.3 vs. 111.2 ± 17.0 and 108.4 ± 26.6; *F* = 3.534, *p* < 0.033*).

MABP values confirmed sufficiently deep anesthesia. MABP slightly elevated during ischemia (83 ± 8 vs. 77 ± 4 mmHg, ischemia vs. baseline) and fell due to transient hypoxia (to 66 ± 8 mmHg), at no statistical significance over the experimental protocol (*F* = 3.349, *p* < 0.127). DMT application had no discernible impact on MABP (*F* = 0.125, *p* < 0.738) (Fig. 2a). Heart rate was stable throughout the experimental protocol (e.g. vehicle group: 331 ± 27, 327 ± 41 and 319 ± 43 bpm, baseline, ischemia and reperfusion; *F* = 0.012, *p* < 0.918). DMT elevated heart rate slightly but not significantly (e.g. reperfusion: 344 ± 19 vs. 319 ± 43 bpm, DMT vs. vehicle; *F* = 1.290, *p* < 0.307).

Any consequence of DMT application on baseline CBF variation was also considered. After ischemia induction, CBF dropped sharply and then stabilized at 40.3 ± 4.8% prior to SD1, and at 34.2 ± 10.1% prior to the induction of transient hypoxia in the vehicle-treated group (Fig. 2b). With hypoxia, perfusion decreased further (to 28.3 ± 5.4%). Reactive hyperemia was not obvious as reperfusion was imposed; instead, CBF peaked at 70.1 ± 17.8%. DMT did not alter baseline CBF at any time point or condition considered (Fig. 2b).

3.2. The impact of DMT on the evolution of spreading depolarization

As the suppression of spontaneous, recurrent SDs by pharmacological means has emerged as a promising target in ischemic neuroprotection (Klass et al., 2018; Szabó et al., 2019; Varga et al., 2020), we have sought to explore the SD limiting potential of DMT. We have also aimed to tackle by pharmacological means whether DMT action may be achieved via Sig-1R activation.

The amplitude of SD was significantly reduced in the presence of DMT (−16.5 ± 4.1 vs. −20.1 ± 1.3 mV, DMT vs. vehicle) (Fig. 3a–b).

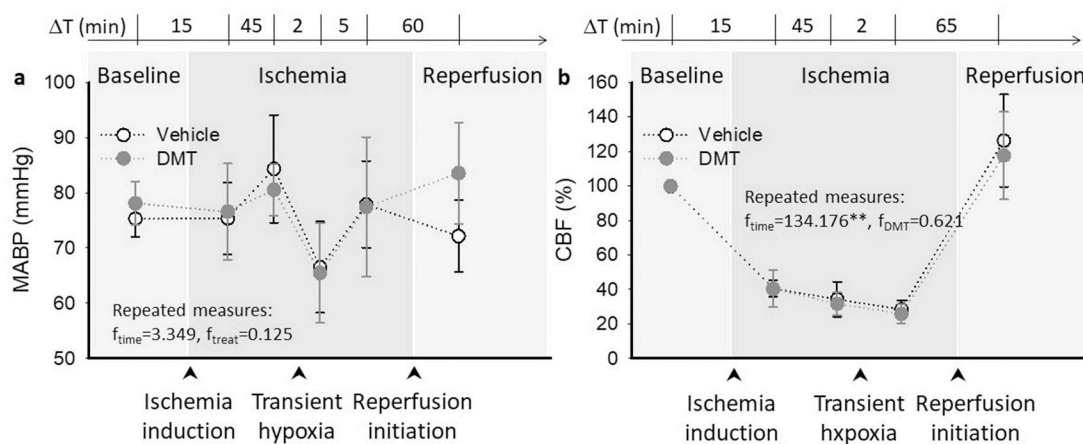


Fig. 2. Mean arterial blood pressure (MABP) and cerebral blood flow (CBF) variations over the experimental protocol. **a**, DMT exerted no impact on MABP over the experimental protocol. **b**, While CBF was obviously reduced during ischemia, DMT did not change the CBF baseline variations with respect to the vehicle group. In “a” and “b”, data are given as mean ± stdev. A repeated measures model was used for statistical analysis (*p* < 0.05* and *p* < 0.01**).

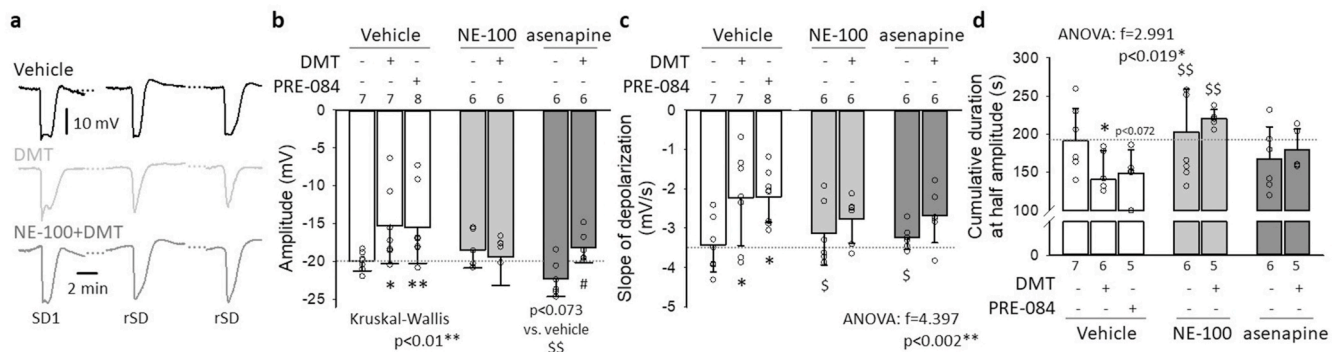


Fig. 3. The impact of pharmacological treatments on the electrophysiological features of spreading depolarization (SD). **a**, Representative traces demonstrate that DMT treatment progressively attenuated the amplitude of subsequent SD events compared to vehicle-treated control, which action was prevented by the co-application of the Sig-1R antagonist NE-100. **b**, Similar to DMT, the highly specific Sig-1R agonist PRE-084 also decreased the amplitude of SDs. NE-100 co-application with DMT diminished DMT action. DMT co-applied with the broad-spectrum serotonin receptor antagonist asenapine achieved SD amplitude reduction compared to asenapine application alone. Data are given as mean \pm stdev. The number of animals (mean of 3 SD events per animal) is indicated in each bar. The test of normality indicated that the distribution of data was not normal (Shapiro-Wilk test: $df = 46$ $p = 0.001^{**}$). Consequently, a Kruskal-Wallis H test was applied ($p < 0.01^{**}$), followed by an independent-samples Mann-Whitney U test ($p < 0.05^*$ and $p < 0.01^{**}$ vs. vehicle alone, $p < 0.01^{SS}$ vs. DMT alone, $p < 0.05^{\#}$ vs. asenapine alone). **c**, DMT and PRE-084 administration also decreased the rate of depolarization, which was prevented by both NE-100 and asenapine. **d**, DMT and PRE-084 reduced the cumulative duration of SD events, while NE-100 (alone or in combination with DMT) exhibited the opposite effect. In “c-d”, data are given as mean \pm stdev. The number of animals (mean of 3 SD events per animal) is indicated in each bar. Statistical analysis indicated a normal distribution of data (c: Shapiro-Wilk test: $df = 46$ $p = 0.360$; d: Shapiro-Wilk test: $df = 40$ $p = 0.383$), therefore the analysis proceeded with a one-way ANOVA paradigm followed by a Fisher (least significant difference, LSD) post hoc test ($p < 0.05^*$ vs. vehicle alone, $p < 0.05^{\$}$ and $p < 0.01^{SS}$ vs. DMT/PPRE-084 alone).

Likewise, the rate of depolarization proved to be also slower in the DMT-treated group with respect to control (-2.62 ± 1.28 vs. -3.48 ± 0.94 mV/s, DMT vs. vehicle) (Fig. 3c). Finally, the cumulative duration of SD events was shortened in the DMT-treated group (140 ± 38 vs. 191 ± 42 s, DMT vs. vehicle) (Fig. 3d).

The share of Sig-1R activation in DMT-linked SD attenuation was explored by the application of a highly selective Sig-1R agonist PRE-084, or the use of a Sig-1R antagonist NE-100 alone or in combination with DMT. In the presence of PRE-084, the DMT-related reduction of SD amplitude and slower rate of depolarization were replicated (i.e. amplitude: -16.2 ± 5.6 vs. -20.1 ± 1.3 mV, PRE-084 vs. vehicle; rate of depolarization: -2.26 ± 1.06 vs. -3.48 ± 0.94 mV/s, PRE-084 vs. vehicle) (Fig. 3b-c), and the cumulative duration of SDs also tended to be shorter (149 ± 31 vs. 191 ± 42 s, PRE-084 vs. vehicle). NE-100 alone did not cause any notable change in SD amplitude, rate of depolarization or cumulative duration (e.g. amplitude: -18.7 ± 2.6 vs. -20.1 ± 1.3 mV, NE-100 vs. vehicle) (Fig. 3b-d). In contrast with DMT applied alone, the co-application of NE-100 and DMT did not achieve any meaningful reduction of SD amplitude (-19.2 ± 4.5 vs. -20.1 ± 1.3 mV, NE-100+DMT vs. vehicle), depolarization rate (-3.06 ± 1.18 vs. -3.48 ± 0.94 mV/s, NE-100+DMT vs. vehicle), or cumulative duration (220 ± 12 vs. 191 ± 42 s, NE-100+DMT vs. vehicle) either (Fig. 3b-d).

Next, we considered the possibility that DMT may activate 5-HTRs (Caronaro and Gatch, 2016) and thereby inhibit SD (Guedes et al., 2017). To this end, we administered the broad spectrum 5-HTR antagonist asenapine (Shadid et al., 2009) alone or co-applied with DMT. The amplitude of SD was significantly greater in the presence of asenapine alone as compared with vehicle (-22.6 ± 2.6 vs. -20.1 ± 1.3 mV, asenapine vs. vehicle). The co-application of DMT with asenapine re-established SD amplitude to control level (-19.1 ± 1.3 vs. -22.6 ± 2.6 mV, asenapine + DMT vs. asenapine) (Fig. 3b). The relative amplitude of SD was greater in asenapine + DMT group with respect to DMT alone (-22.6 ± 2.6 vs. -16.5 ± 4.1 mV), albeit the difference was statistically not significant. These data collectively suggest that the SD-suppressing action of DMT was likely realized, at least in part, via Sig-1R activation.

Of the three subsequent elements of the CBF response to SD (i.e. brief transient hypoperfusion, transient peak and late hyperemia, and long-lasting oligemia) (Ayata and Lauritzen, 2015) our analysis predominantly focused on the phase of hyperemia, which evolved reliably with

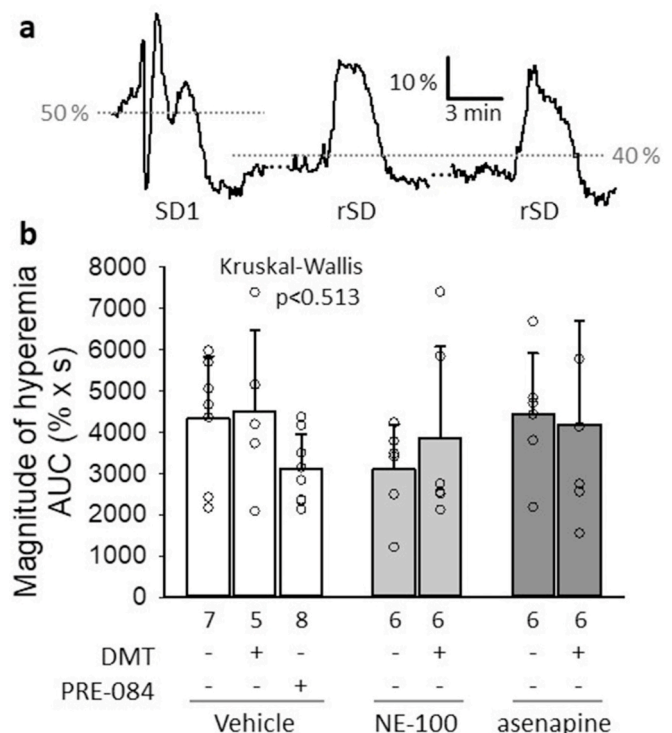


Fig. 4. The impact of pharmacological treatments on the cerebral blood flow (CBF) response to spreading depolarization (SD). **a**, A trace representative of the vehicle group depicts the CBF response to the first (SD1) and recurrent SDs (rSD), as acquired with laser-Doppler flowmetry. **b**, The area under the curve (AUC) of the hyperemic component of the CBF response represents the magnitude of SD-related hyperemia, which was not modulated by any of the pharmacological treatments. Data are given as mean \pm stdev. The number of animals (mean of 3 SD events per animal) is given in each bar. The test of normality indicated that the distribution of data was not normal (Shapiro-Wilk test: $df = 44$ $p = 0.031^*$). Consequently, a Kruskal-Wallis H test was applied.

each SD (Fig. 4a). We narrowed down our analysis to recurrent SDs, because the kinetics of the CBF response to the first SD in a train is substantially different from the response given to recurrent SDs (Farkas et al., 2008; Ayata and Lauritzen, 2015) (Fig. 4a).

In our experiments, the CBF response to recurrent SDs appeared to be resistant to all of the used pharmacological agents, including DMT or the selective Sig-1R agonist PRE-084. Like other parameters (i.e. amplitude or duration of hyperemia), the magnitude of hyperemia characterized by the area under the curve (AUC) was similar across various treatment regimes (Fig. 4b).

3.3. Neuroprotection achieved with DMT

Neuronal survival has been characterized by the surface area occupied by NeuN-labeled neurons relative to the full field of view, in the somatosensory cortex and the hippocampus (Fig. 5a). With respect to naïve animals, no significant difference in NeuN immunopositivity was noted due to ischemia/hypoxia/reperfusion (e.g. somatosensory cortex: 19.9 ± 1.9 vs. $19.3 \pm 1.4\%$, vehicle vs. naïve). Neuronal loss that might have been associated with SD was not found, either (e.g. somatosensory cortex: 19.5 ± 3.1 vs. $20.2 \pm 3.2\%$, ipsi-vs. contralateral side to SD). Finally, DMT treatment exerted no meaningful effect on NeuN labeling (e.g. contralateral somatosensory cortex: 17.4 ± 2.0 vs. $19.9 \pm 1.9\%$, DMT vs. vehicle).

As neurons in the hippocampus CA1 and dentate gyrus (DG), the most vulnerable regions to ischemia are packed with pericarya so tightly that NeuN staining may not reveal individual cell loss, we labeled cells engaged in apoptotic cell death with CC3 immunostaining (Fig. 5b).

Sections from naïve animals were virtually devoid of CC3-positive cells (i.e. DG: 163 ± 14 CC3+ cells per mm^2), while CC3 labeled cell bodies were obvious in the cortex, hippocampus CA1 region, and particularly in the DG after ischemia/hypoxia/reperfusion in the vehicle group (DG: 1649 ± 278 CC3+ cells per mm^2) (Fig. 5b). The aggravation of apoptosis by recurrent SDs was anticipated in the cortex, where SDs propagated (Jahanbazi et al., 2018), but no lateralization of CC3 cell count was detected (vehicle group: 106 ± 46 vs. 104 ± 67 CC3+ cells per mm^2 , ipsi-vs. contralateral). For this reason, CC3+ cell counts obtained from the two hemispheres were averaged for each region. Importantly, significantly fewer CC3 labeled apoptotic cells were counted in the DMT-treated compared to vehicle-treated animals in the somatosensory cortex (66 ± 33 vs. 105 ± 56 CC3+ cells per mm^2 , DMT vs. vehicle), hippocampal CA1 region (532 ± 268 vs. 893 ± 249 CC3+ cells per mm^2 , DMT vs. vehicle) and DG (1367 ± 311 vs. 1649 ± 278 CC3+ cells per mm^2 , DMT vs. vehicle) (Fig. 5b).

In addition to apoptosis, ischemic/hypoxic stress may induce ferroptosis, an alternative pathway of programmed cell death that has been recognized recently (Dolma et al., 2003; Stockwell et al., 2017). The typical hallmark of ferroptosis is the iron-dependent accumulation of lipid hydroperoxides, hence the cellular process can be detected by 4-HNE immunohistochemistry (Cao and Dixon, 2016). Ferroptosis was obvious in selected neurons in the hippocampus CA1 and dentate gyrus (Fig. 5c). The number of ferroptotic cells tended to be lower in the DMT-treated CA1 (4.53 ± 0.39 vs. 6.13 ± 2.49 count/ mm^2 , DMT vs. vehicle), but this difference was statistically not significant. Also, the cell counting approach was not fully reliable due to the cell density in the CA1 pyramidal cell layer and the dentate gyrus granule cell layer (i.

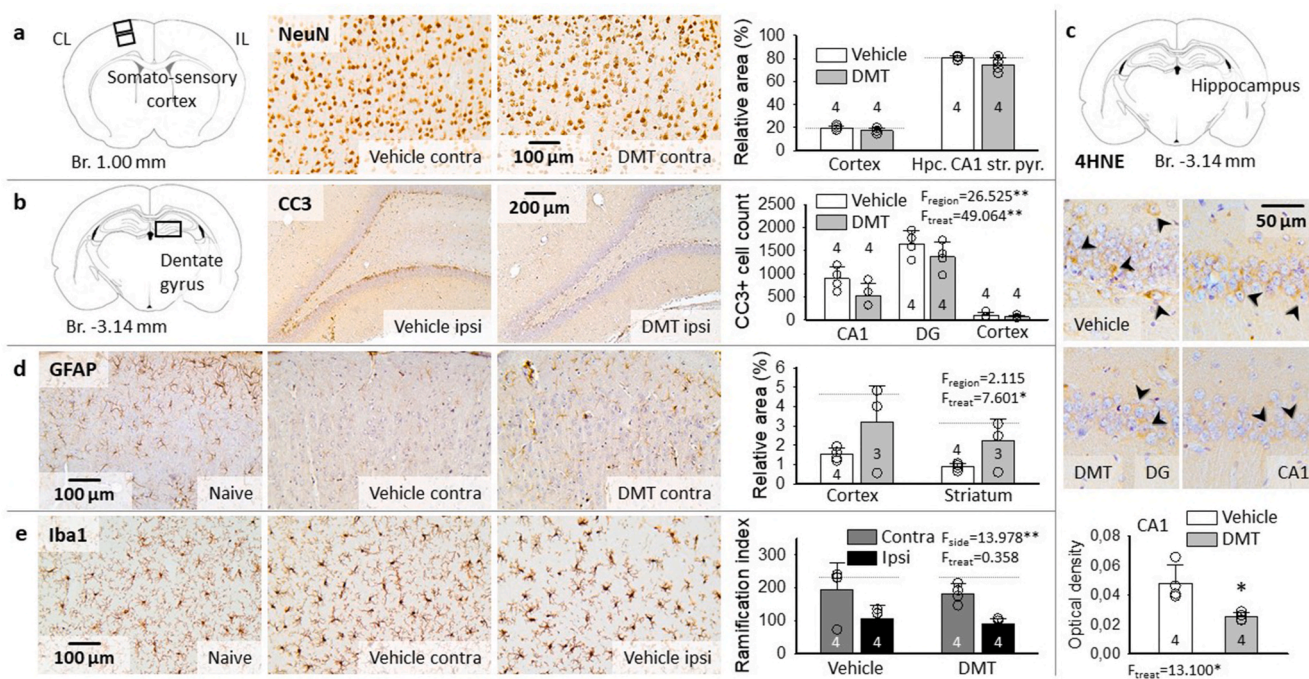


Fig. 5. Representative light microscopic images of immuno-labeled sections and bar charts demonstrate neuroprotection achieved by DMT administration in cortical (sensory cortex and hippocampus) and subcortical gray matter (striatum). **a**, No changes were observed in the density of NeuN-labeled neurons, either due to ischemia/reperfusion, or DMT treatment. **b**, Cleaved caspase-3 (CC3) positive apoptotic cells in the granule cell layer of the dentate gyrus (DG) were obvious, and were also present to a lesser degree in the hippocampus CA1 region after ischemia/reperfusion in the vehicle group. DMT administration reduced the number of CC3-positive apoptotic cells. Cell count is given for 1 mm^2 surface area. **c**, Representative sections labeled for 4-hydroxynonenal (4-HNE) indicate ferroptotic cell death (arrowheads) in the hippocampus dentate gyrus (DG, image pair to the left) and CA1 region (image pair to the right). Note that even though the number of 4-HNE-positive cells was not significantly different between experimental groups, the optical density of the perinuclear cytoplasm was considerably lower after DMT treatment (bar chart below). **d**, Glial fibrillary acidic protein (GFAP)-positive astrocytes were lost following ischemia/reperfusion in the vehicle group, but were partially rescued by DMT treatment. **e**, Prominent microglia activation was detected in the cortex ipsilateral to SD-elicitation and the craniotomies (M. Tóth et al., 2020), which was not modulated by DMT application. In the bar charts of Panels “a-d”, data are presented as mean \pm stdev, sample size is given in each bar. Horizontal dotted lines indicate levels measured in naïve rats ($n = 3$). Statistical analysis was conducted using a one-way (e.g. 4-HNE) or two-way ANOVA model with treatment and region (e.g. NeuN, GFAP, CC3), or side and treatment (Iba-1) as factors ($p < 0.05^*$; $p < 0.01^{**}$).

e. discriminating individual cells carries uncertainty). However, the lower intensity of the 4-HNE staining in the perinuclear cellular cytoplasm after DMT treatment was conspicuous and indicated an anti-ferroptotic effect of DMT (0.025 ± 0.002 vs. 0.048 ± 0.012 , DMT vs. vehicle) (Fig. 5c).

Because astrocytes have been widely known to support neuronal function under ischemia (Rossi et al., 2007), and GFAP-positive protoplasmic astrocytes may become selectively vulnerable to ischemic conditions (Lukaszevicz et al., 2002), we have explored whether DMT has the potential to protect astrocytes. We used GFAP immunocytochemistry to label astrocytes (Fig. 5d). The relative area occupied by GFAP immunolabeled compartments considerably decreased after ischemia/hypoxia/reperfusion compared to naive animals, which reduction was counteracted by DMT-treatment in the cortex and striatum (cortex: 3.2 ± 1.9 vs. 1.5 ± 0.3 vs. $4.7 \pm 0.9\%$, striatum: 2.3 ± 1.1 vs. 0.9 ± 0.2 vs. $3.2 \pm 1.6\%$, DMT vs. vehicle vs. naive), but not in the hippocampus (i.e. CA1 stratum oriens 10.6 ± 4.9 vs. 11.1 ± 5.8 vs. $15.5 \pm 2.7\%$, DMT vs. vehicle vs. naive) (Fig. 5d).

Ischemic insults trigger microglial activation and neuro-inflammatory reaction that may be modulated via Sig-1Rs (Szabo et al., 2016; Jia et al., 2018). In the cerebral cortex ipsilateral to the craniotomies and SD initiation, decreasing microglial arborization was expected to denote the amplification of microglial activation (Varga et al., 2020; M. Tóth et al., 2020). The current data confirm the previous observations by showing less dense microglia ramification in the ipsilateral cortex compared to the contralateral side (vehicle group: 106.6 ± 50.5 vs. 194.3 ± 95.6 , ipsi-vs. contralateral) (Fig. 5e). Yet, the administration of DMT did not exert any distinguishable effect on the microglial ramification index (i.e. ipsilateral cortex: 89.5 ± 37.4 vs. 106.6 ± 50.5 DMT vs. vehicle) (Fig. 5e).

3.4. Receptor binding, tissue DMT content and Sig-1R co-localization

The binding affinities of the compounds for the Sig-1R were determined in competitive binding assays. The assay conditions were validated with various Sig-1R ligands and the following order of potency for Sig-1R binding was found: (+)-pentazocine > fluvoxamine > PRE-084 (Fig. 6a). All three compounds exhibited nanomolar Sig-1R affinities and induced a similar maximal displacement (around 90–100%). To evaluate if DMT exerts its action by binding to Sig-1R, the Sig-1R binding affinity of DMT was investigated in the absence or presence of asenapine, a potent serotonin- and dopamine receptor antagonist (Shadid et al., 2009).

Competition binding assays in rat brain membrane homogenate against the Sig-1R specific radioligand [^3H](+)-pentazocine revealed that DMT bound the Sig-1R with an inhibitory constant value of $15.1 \mu\text{M}$. This is in agreement with the results of Fontanilla et al. (2009), who found that DMT bound the Sig-1R at low micromolar concentrations ($K_d = 14.7 \mu\text{M}$) in guinea pig liver membrane homogenate. Asenapine could not displace the radioligand from the [^3H](+)-pentazocine binding sites ($10 \mu\text{M}$ asenapine reduced total specific binding of the radioligand to 82%) indicating the lack of specific affinity of asenapine for the Sig-1R (Fig. 6a₁). When $10 \mu\text{M}$ asenapine was added to DMT, no significant difference was observed in the Sig-1R binding affinity of DMT, indicating that asenapine did not influence the Sig-1R binding of DMT (Fig. 6a₂).

Since DMT is rapidly degraded by monoamine oxidases (MAO) in peripheral tissues (Burchett and Hicks, 2006), we evaluated blood plasma and brain tissue DMT content with 2D-LC-MS/MS (Körmöczsi et al., 2020). Importantly, DMT administered at a dose of 1 mg/kg/h by i.v. infusion was clearly detectable in blood plasma measured 50 min

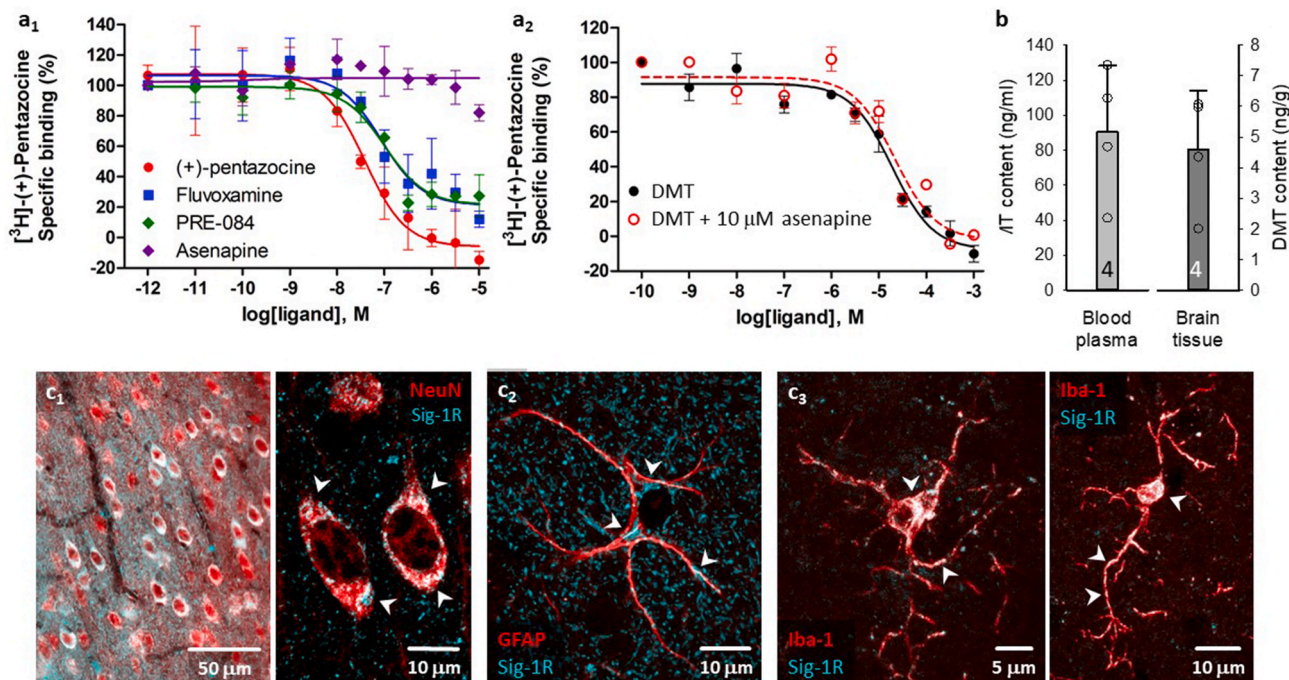


Fig. 6. Sig-1R ligand binding affinities in rat brain homogenates, blood plasma and brain tissue DMT content, and the cellular localization of Sig-1R in the rat cerebral cortex. **a**, Competitive binding curves of various Sig-1R ligands against the radioactive Sig-1R ligand [^3H](+)-pentazocine (A₁) and of DMT in the absence or presence of $10 \mu\text{M}$ asenapine (A₂) in rat brain membrane homogenates. Curves are shown as percent specific binding ($10 \mu\text{M}$ haloperidol). **b**, Blood plasma and brain tissue were enriched in DMT after intravenous infusion, as measured by two-dimensional liquid chromatography coupled to quadrupole-Orbitrap mass spectrometry (2D-LC-MS/MS). In contrast, DMT was undetectable in blood plasma and brain tissue of control rats by 2D-LC-MS/MS (data not shown). **c**, Immuno-labeled brain slices demonstrate the perinuclear localization of Sig-1R in NeuN-labeled cortical pyramidal cells (epifluorescent and confocal microscopic images; c₁). In GFAP-positive astrocytes, Sig-1R was seen in the perinuclear soma, and in processes (confocal microscopic image; c₂). Both the soma and processes of Iba-1-labeled microglia were endowed with Sig-1Rs (confocal microscopic image; c₃).

after the initiation of DMT infusion (90.5 ± 37.9 ng/mL, ca. $0.5 \mu\text{M}$), and in the brain tissue sampled upon the termination of the experimental protocol (4.6 ± 1.9 ng/g tissue, ca. $0.02 \mu\text{mol/kg}$) (Fig. 6b). Potential endogenous DMT concentration in the vehicle group remained below detection level.

Finally, to identify cell types that may be targeted by DMT, we co-localized Sig-1R with neurons, astrocytes, and microglia with fluorescent immunocytochemistry in naïve rats. Sig-1Rs were expressed abundantly in neurons (Fig. 6c₁), and were also associated with astrocytes (Fig. 6c₂), and resting microglia (Fig. 6c₃).

4. Discussion

The objective of our current study was to explore whether DMT administration achieves neuroprotection via Sig-1R activation in the acute phase of experimental, transient, cerebral forebrain ischemia, aggravated by the recurrent induction of SDs and a subsequent transient hypoxic episode. DMT is a natural, endogenous Sig-1R ligand, which is thought to pose as an advantage of DMT application as opposed to other, synthetic Sig-1R agonists.

The impact of DMT treatment on physiological variables was screened comprehensively, because single intravenous doses of DMT have been reported to cause sympathetic activation, and to prominently increase blood pressure and heart rate within minutes after administration (Strassman and Qualls, 1994). In our experiments, DMT exerted no obvious impact on cardiovascular or cerebrovascular function (Fig. 2), which may be attributed to the continuous, slow infusion of DMT (rather than a bolus application), controlled anesthesia, or their combination. The absence of apparent cardio- or cerebrovascular effects in our study proved to be favorable, as the neuroprotective potential of DMT could be assessed free of any marked changes in physiological variables.

Recurrent SD events have served here the evaluation of the ischemic neuroprotective potential of DMT, linked to Sig-1R activation. SD is the synchronized depolarization of a critical bulk of tissue in the cerebral gray matter, which is thought to be triggered by local metabolic supply-demand mismatch under ischemia (von Bornstädt et al., 2015). SD propagates over the cerebral cortex at a slow rate of a few mm/min, by progressively involving neighboring tissue in the depolarization (Leao, 1944; Somjen, 2001). Further, SD is accompanied by a CBF response dominated typically by a remarkable hyperemic element (Fig. 4a), which serves the replenishment of ATP necessary for timely repolarization behind the SD wave front (Ayata and Lauritzen, 2015). Importantly, recurrent SDs have been recognized as a universal principle of lesion progression in the injured cerebral gray matter (Hartings et al., 2017; Dreier et al., 2017)], and SD suppression has been considered as a promising therapeutical approach to improve neurological outcome after acute brain injury (Carlson et al., 2018, 2020; Klass et al., 2018).

In our current experiments, SD amplitude, the rate of depolarization and cumulative SD duration were reduced under intravenous DMT administration, exhibiting the SD limiting impact of DMT. Further, the application of the selective Sig-1R agonist PRE-084 reproduced the SD hampering action of DMT, and the Sig-1R antagonist NE-100 co-applied with DMT diminished the DMT-related SD inhibition (Fig. 3). These results collectively suggest that DMT may impede SD evolution by Sig-1R activation. The implication of Sig-1Rs is supported by previous reports demonstrating that dextromethorphan or carbetapentane – two ligands known as Sig-1R agonists – reproducibly and reliably blocked SD occurrence in live brain slice preparations (Anderson and Andrew, 2002; Anderson et al., 2005; Church et al., 2005).

Recurrent SDs may accelerate ischemic lesion maturation because SD is associated with an intracellular rise of calcium (Siesjö and Bengtsson, 1989; Reinhart and Shuttleworth, 2018), which potentially contributes to the calcium overload known to initiate ischemic neurodegeneration (Szydłowska and Tymianski, 2010). Indeed, the non-competitive NMDA receptor antagonist ketamine inhibited SD evolution with a concomitant

reduction of neuronal calcium content in brain slice preparations (Reinhart and Shuttleworth, 2018), and voltage-gated calcium channel blockers reduced SD amplitude in anesthetized rats (Richter et al., 2002; Szabó et al., 2019), similar to that seen here. Intriguingly, Sig-1R agonism was shown to attenuate the NMDA receptor activation-linked calcium response in cultured neurons (Klette et al., 1997), and to depress calcium currents with a corresponding inactivation of neuronal voltage-gated calcium channels (Zhang et al., 2002). On the basis of these and our experimental data together, we postulate that DMT in our experiments possibly inhibited SD via Sig-1R-linked modulation of intracellular calcium homeostasis.

The suggestion that DMT predominantly achieved SD inhibition by Sig-1R activation – rather than through 5-HTR binding (Yanaí et al., 1986; Deliganis et al., 1991) – is also substantiated by our finding that DMT counteracted the SD potentiating effect of asenapine (Fig. 3), an antagonist of multiple 5-HTRs (Shahid et al., 2009). In other words, when 5-HTRs were occupied by asenapine, DMT still reduced SD amplitude with respect to the condition when asenapine was given alone. Of note, our results that 5-HTR antagonism increased SD amplitude (Fig. 3) are complementary to previous reports showing that ablation of the dorsal raphe serotonergic neurons accelerated SD propagation in the cerebral cortex (Cui et al., 2013), electrical stimulation of the dorsal raphe or the administration of sumatriptan, a 5-HT_{1D} receptor agonist decelerated SD (Guedes et al., 2017), and sumatriptan also suppressed SD evolution in experimental focal cerebral ischemia (Mies et al., 1998). Thus, serotonergic activity appears to restrain SD, and, conversely, serotonergic deficiency may augment SD.

Finally, we evaluated the impact of the pharmacological treatments on the CBF response to SD, especially because it is unknown whether and how DMT might alter neurovascular coupling. Another consideration has been that the CBF response to SD in the hypoperfused cerebral cortex is understood to be insufficient to meet the metabolic demand of the nervous tissue (Dreier, 2011; Hoffmann and Ayata, 2013), therefore the pharmacological enhancement of the SD-associated CBF response may support neuronal survival in tissue at risk (Dreier et al., 1998; Varga et al., 2020). DMT treatment in our experiments, however, did not alter the SD-related hyperemia (Fig. 4). Furthermore, none of the other agents used (the Sig-1R agonist PRE-084, the Sig-1R antagonist NE-100 or the 5-HTR antagonist asenapine) proved to be effective at modulating the SD-associated CBF response in any meaningful way (Fig. 4). The implication of Sig-1R in the mediation of the SD-associated hyperemia has been previously unattended, and our current results do not support the notion that Sig-1R signaling may augment the SD-related CBF response, at least not under ischemic conditions. On the other hand, the 5-HT_{1D/1B} receptor agonist zolmitriptan increased, while the 5-HT_{2A/2C} receptor antagonist ritanserin attenuated the amplitude of hyperemia in the optimally perfused cerebral cortex (Gold et al., 1998). The non-specific 5-HTR antagonist asenapine would then be expected to curb the hyperemic response to SD, but exerted no effect. The condition that SDs occurred here in ischemic tissue could have possibly overridden physiological blood flow regulation with SD (Varga et al., 2016) – indeed, ischemia is known to impair neurovascular coupling (Jackman and Iadecola, 2015). Taken together, we assume that Sig-1R or 5-HTR-based modulation of the CBF response to SD in the ischemic cerebral cortex proves to be ineffective.

Several groups have reported independently that Sig-1R agonism successfully reduced infarct size estimated 24 h or a number of days after an episode of experimental focal cerebral ischemia (Ajmo et al., 2006; Omi et al., 2014; Sato et al., 2014; Nardai et al., 2020). Therefore, we proceeded to investigate the neuroprotective potential of DMT at histological level as early as 2 h after ischemia induction and 1 h after reperfusion initiation (Fig. 1). In our experiments, NeuN staining did not reveal significant loss of neurons, possibly because the end point was too early to detect massive neurodegeneration (i.e. infarct maturation), and the staining is too dense to be sensitive for the selective loss of scattered, individual cells. However, the network of GFAP-positive astrocytes

became remarkably sparser after ischemia/reperfusion as compared to naïve samples (Fig. 5d). This is consistent with the loss of the GFAP signal and swelling of protoplasmic astrocytes in the first hours after the onset of experimental focal cerebral ischemia, suggestive of astrocyte dysfunction (Lukaszewicz et al., 2002). Importantly, the GFAP signal has been partially restored in our experiments when DMT was administered and Sig-1R co-localized with astrocytes (Fig. 6c), which is complementary to a previous report demonstrating that Sig-1R agonism augmented astrocyte survival screened 96 h after ischemia onset (Katnik et al., 2016). These results indicate that DMT preserved the integrity of the astrocyte network – and presumably function – by Sig-1R receptor activation.

The labeling of microglia replicated our previous results that microglia activation – characterized by the less dense arborization of microglial processes – appeared more pronounced in the cortex ipsilateral to SD elicitation (Fig. 5e) (Tóth et al., 2020; Varga et al., 2020). As we argued previously, the recurrence of SDs and the procedure of trepanation both contribute to the enhanced activation of microglia (Tóth et al., 2020; Varga et al., 2020). DMT has emerged to curtail inflammatory responses, substantiated by the reduced production of pro-inflammatory cytokines by provoked human primary monocyte-derived dendritic cells (Szabo et al., 2014), and the lower pro-inflammatory cytokine serum levels in rats suffering of stroke (Nardai et al., 2020). Moreover, Sig-1R agonism with 1,3-di-(2-tolyl) guanidine (DTG) inhibited the activation and cytokine release of cultured microglia provoked by endotoxin (Hall et al., 2009). These data and the expression of Sig-1R in microglia (Fig. 6) (Nardai et al., 2020) led to the assumption that DMT treatment may target microglia. Yet, in the current experiments, DMT had no discernible impact on microglia activation (Fig. 6c). Likewise, Sig-1R activation achieved no change in Iba-1 immuno-labeling and cerebral cytokine production in a focal cerebral ischemia model (Ruscher et al., 2012). Taken together, we propose that DMT treatment may suppress the activation of dendritic cells or microglia provoked with direct inflammatory stimuli in culture, but may not be as potent to inhibit microglia activation caused by ischemia or SD in anesthetized rodents.

Apoptotic cell death has emerged as an especially relevant target to investigate, because Sig-1R agonism has been revealed to suppress ER stress-related apoptosis (Omi et al., 2014; Sato et al., 2014; Zhao et al., 2019). Concurring with the evidence that DMT activates Sig-1Rs (Fontanilla et al., 2009), and in line with the above data on the anti-apoptotic effect of Sig-1R activation, DMT treatment reduced here the number of CC3-positive apoptotic cells, especially in the hippocampus. On the basis of their histological position, a fraction of these cells must have been neurons (Fig. 5b), which cell type is endowed with Sig-1Rs (Fig. 6c). The early activation of CC3 here must be attributed to the ischemia/reperfusion and anoxia rather than SD, because we did not identify any lateralization of apoptosis that would correspond to SD. This is consistent with previous findings that the incomplete global forebrain ischemia model is sufficient alone to produce neuronal injury (Farkas et al., 2007). The time course of caspase activation is expected to vary around 15–30 min as measured in single cells (HeLa D98 cells) in culture (Rehm et al., 2002), but may exceed this time dependent on the stimulus in neuron populations *in vivo* (Teschendorf et al., 2008). It is plausible that the time window taken here is too short to appreciate the impact of SD on CC3 activation and its pharmacological inhibition in the otherwise ischemic brain tissue.

Similar to the impact of DMT treatment on apoptosis, our 4-HNE staining showed that DMT administration reduced the intensity of ferroptosis, as well (Fig. 5c). It is a novel observation, consistent with the finding that Sig-1R activation or overexpression inhibits the generation of reactive oxygen species (Hayashi, 2019).

Finally, in support of our *in vivo* functional and histological results, we set out to test DMT binding affinity to rat cerebral Sig-1R, because the reference assay we relied on had been conducted on guinea pig liver homogenates (Fontanilla et al., 2009). Our competition binding assay

revealed that DMT bound cerebral Sig-1R at an inhibitory constant value of 15.1 μM , which corresponds to that measured in guinea pig liver membrane homogenates ($K_d = 14.7 \mu\text{M}$) (Fontanilla et al., 2009), and substantiates our *in vivo* pharmacological data with confidence. We also measured the DMT content of blood plasma and brain homogenates to confirm that DMT was present to exert biological effects. Previously we reported that our analytical method was not sensitive enough to detect endogenous DMT, but was reliable to measure exogenous tissue DMT content (Körmöczí et al., 2020). Here, we successfully confirmed the presence of exogenous DMT in our samples in the range of 4–90 ng/g or ng/mL sample (ca. 0.02 $\mu\text{mol/kg}$ for brain or 0.5 μM for plasma; Fig. 6b). Since, due to receptor reserves, fractional occupancy of a receptor pool may still generate a maximal biological effect, the micromolar Sig-1R affinity of DMT may be sufficient to elicit a Sig-1R mediated effect at the measured DMT concentrations, especially in the presence of the off-target antagonist asenapine. It was also found that asenapine did not bind to Sig-1R and did not influence the Sig-1R binding of DMT. The DMT content in our samples is most probably an underestimation of the true concentration, because DMT must have been rapidly degraded during the procedure of harvesting samples (Burchett and Hicks, 2006), especially when extracting brain tissue (i.e. the half-life of DMT was found to be 5–6 min in rat brain tissue) (Sitaram et al., 1987).

In conclusion, here we present novel observations that DMT administered with therapeutic purpose in the early phase of cerebral ischemia impedes the evolution of recurrent SDs, which are known to jeopardize the survival of viable penumbra tissue in ischemic stroke (Mies, 1998; Hartings et al., 2017). Further, we demonstrate that DMT protects astrocytes against ischemic injury, and suppresses ischemia/reperfusion-related apoptosis in the nervous tissue. As an original observation, we show that DMT appears to counteract ferroptotic cell death linked to oxidative stress. Finally, we have accumulated compelling evidence that DMT most likely achieves its neuroprotective effect via Sig-1R activation. The beneficial effects of DMT manifested at regular cardiovascular function and unreturned cerebral perfusion. Overall, our data support the notion, that the timely administration of DMT may be considered as an adjuvant pharmacological therapy in the treatment of acute cerebral ischemic injury (Szabo and Frecska, 2016), especially because of reported low risk of toxicity (Carbonaro and Gatch, 2016).

Funding

This work was supported by grants from the National Research, Development and Innovation Office of Hungary (K134377 to EF; K120358 to FB, K124952 to CT, FK135425 to AEF, and PD128821 to ÁM); the Ministry of Human Capacities of Hungary (NTP-NFTÖ-20-B-0016 to VÉV, ÚNKP-19-3-SZTE-266 to ÍS, ÚNKP-19-3-SZTE-81 to RF and ÚNKP-19-4-SZTE-43 to AEF); the Economic Development and Innovation Operational Programme in Hungary co-financed by the European Union and the European Regional Development Fund (No. GINOP-2.3.2-15-2016-0006 to EF), the EU-funded Hungarian grant No. EFOP-3.6.1-16-2016-00008 to EF, and University of Szeged Open Access Fund (nr. 5327).

Author contributions

ÍS: Conceptualization, Data curation, Formal analysis, Writing - original draft; VÉV, SD, AEF, TK, RB, RF, DH, CT: Data curation; Formal analysis; ÁM: Methodology; NVC, EFr, IAK, FB: Conceptualization, Supervision; EFA: Conceptualization, Supervision, Project administration, Writing - original draft.

Declaration of competing interest

The authors declare that they have no known competing financial interests or personal relationships that could have appeared to influence

the work reported in this paper.

Acknowledgements

We are grateful to Professor Botond Penke for invaluable conceptual advice.

References

Ajmo Jr., C.T., Vernon, D.O., Collier, L., Pennypacker, K.R., Cuevas, J., 2006. Sigma receptor activation reduces infarct size at 24 hours after permanent middle cerebral artery occlusion in rats. *Curr. Neurovascular Res.* 3 (2), 89–98. <https://doi.org/10.2174/156720206776875849>.

Anderson, T.R., Andrew, R.D., 2002. Spreading depression: imaging and blockade in the rat neocortical brain slice. *J. Neurophysiol.* 88 (5), 2713–2725. <https://doi.org/10.1152/jn.00321.2002>.

Anderson, T.R., Jarvis, C.R., Biedermann, A.J., Molnar, C., Andrew, R.D., 2005. Blocking the anoxic depolarization protects without functional compromise following simulated stroke in cortical brain slices. *J. Neurophysiol.* 93 (2), 963–979. <https://doi.org/10.1152/jn.00654.2004>.

Ayata, C., Lauritzen, M., 2015. Spreading depression, spreading depolarizations, and the cerebral vasculature. *Physiol. Rev.* 95 (3), 953–993. <https://doi.org/10.1152/physrev.00027.2014>.

Barker, S.A., Monti, J.A., Christian, S.T., 1981. N,N-dimethyltryptamine: an endogenous hallucinogen. *Int. Rev. Neurobiol.* 22, 83–110. [https://doi.org/10.1016/s0074-7742\(08\)60291-3](https://doi.org/10.1016/s0074-7742(08)60291-3).

Barker, S.A., McIlhenny, E.H., Strassman, R., 2012. A critical review of reports of endogenous psychedelic N, N-dimethyltryptamines in humans: 1955–2010. *Drug Test. Anal.* 4 (7–8), 617–635. <https://doi.org/10.1002/dta.422>.

Barker, S.A., Borjigin, J., Lomnicka, I., Strassman, R., 2013. LC/MS/MS analysis of the endogenous dimethyltryptamine hallucinogens, their precursors, and major metabolites in rat pineal gland microdialysate. *Biomed. Chromatogr.* 27 (12), 1690–1700. <https://doi.org/10.1002/bmc.2981>.

Bere, Z., Obrenovitch, T.P., Kozák, G., Bari, F., Farkas, E., 2014. Imaging reveals the focal area of spreading depolarizations and a variety of hemodynamic responses in a rat microembolic stroke model. *J. Cerebr. Blood Flow Metabol.* 34 (10), 1695–1705. <https://doi.org/10.1038/jcbfm.2014.136>.

Blough, B.E., Landavazo, A., Decker, A.M., Partilla, J.S., Baumann, M.H., Rothman, R.B., 2014. Interaction of psychoactive tryptamines with biogenic amine transporters and serotonin receptor subtypes. *Psychopharmacology (Berlin)* 231 (21), 4135–4144. <https://doi.org/10.1007/s00213-014-3557-7>.

Bradford, M.M., 1976. A rapid and sensitive method for the quantitation of microgram quantities of protein utilizing the principle of protein-dye binding. *Anal. Biochem.* 72, 248–254. <https://doi.org/10.1006/abio.1976.9999>.

Bunzow, J.R., Sonders, M.S., Arttamangkul, S., Harrison, L.M., Zhang, G., Quigley, D.I., Darland, T., Suchland, K.L., Pasumamula, S., Kennedy, J.L., Olson, S.B., Magenis, R. E., Amara, S.G., Grandy, D.K., 2001. Amphetamine, 3,4-methylenedioxymethamphetamine, lysergic acid diethylamide, and metabolites of the catecholamine neurotransmitters are agonists of a rat trace amine receptor. *Mol. Pharmacol.* 60 (6), 1181–1188. <https://doi.org/10.1124/mol.60.6.1181>.

Burchett, S.A., Hicks, T.P., 2006. The mysterious trace amines: protean neuromodulators of synaptic transmission in mammalian brain. *Prog. Neurobiol.* 79 (5–6), 223–246. <https://doi.org/10.1016/j.pneurobio.2006.07.003>.

Cao, J.Y., Dixon, S.J., 2016. Mechanisms of ferroptosis. *Cell. Mol. Life Sci.* 73 (11–12), 2195–2209. <https://doi.org/10.1007/s00018-016-2194-1>.

Carbonaro, T.M., Gatch, M.B., 2016. Neuropharmacology of N,N-dimethyltryptamine. *Brain Res. Bull.* 126 (Pt 1), 74–88. <https://doi.org/10.1016/j.brainresbull.2016.04.016>.

Carlson, A.P., Abbas, M., Alunday, R.L., Qeadan, F., Shuttleworth, C.W., 2018. Spreading depolarization in acute brain injury inhibited by ketamine: a prospective, randomized, multiple crossover trial. *J. Neurosurg.* 25, 1–7. <https://doi.org/10.3171/2017.12.JNS171665>.

Carlson, A.P., Alchbli, A., Hänggi, D., Macdonald, R.L., Shuttleworth, C.W., 2020. Effect of locally delivered nimodipine microparticles on spreading depolarization in aneurysmal subarachnoid hemorrhage. *Neurocritical Care.* <https://doi.org/10.1007/s12028-020-00935-1>.

Christian, S.T., Harrison, R., Quayle, E., Pagel, J., Monti, J., 1977. The in vitro identification of dimethyltryptamine (DMT) in mammalian brain and its characterization as a possible endogenous neuroregulatory agent. *Biochem. Med.* 18 (2), 164–183. [https://doi.org/10.1016/0006-2944\(77\)90088-6](https://doi.org/10.1016/0006-2944(77)90088-6).

Church, A.J., Andrew, R.D., 2005. Spreading depression expands traumatic injury in neocortical brain slices. *J. Neurotrauma* 22 (2), 277–290. <https://doi.org/10.1089/neu.2005.22.277>.

Cui, Y., Li, Q.H., Yamada, H., Watanabe, Y., Kataoka, Y., 2013. Chronic degeneration of dorsal raphe serotonergic neurons modulates cortical spreading depression: a possible pathophysiology of migraine. *J. Neurosci. Res.* 91 (6), 737–744. <https://doi.org/10.1002/jnr.23209>.

Daumann, J., Wagner, D., Heekeren, K., Neukirch, A., Thiel, C.M., et al., 2010. Neuronal correlates of visual and auditory alertness in the DMT and ketamine model of psychosis. *J. Psychopharmacol.* 24 (10), 1515–1524. <https://doi.org/10.1177/0269881109103227>.

Dean, J.G., Liu, T., Huff, S., Sheler, B., Barker, S.A., et al., 2019. Biosynthesis and extracellular concentrations of N,N-dimethyltryptamine (DMT) in mammalian brain. *Sci. Rep.* 9 (1), 9333. <https://doi.org/10.1038/s41598-019-45812-w>.

Deliganis, A.V., Pierce, P.A., Peroutka, S.J., 1991. Differential interactions of dimethyltryptamine (DMT) with 5-HT1A and 5-HT2 receptors. *Biochem. Pharmacol.* 41 (11), 1739–1744. [https://doi.org/10.1016/0006-2952\(91\)90178-8](https://doi.org/10.1016/0006-2952(91)90178-8).

Dolma, S., Lessnick, S.L., Hahn, W.C., Stockwell, B.R., 2003. Identification of genotype-selective antitumor agents using synthetic lethal chemical screening in engineered human tumor cells. *Canc. Cell* 3 (3), 285–296. [https://doi.org/10.1016/s1535-6108\(03\)00050-3](https://doi.org/10.1016/s1535-6108(03)00050-3).

Dreier, J.P., 2011. The role of spreading depression, spreading depolarization and spreading ischemia in neurological disease. *Nat. Med.* 17 (4), 439–447. <https://doi.org/10.1038/nm.2333>.

Dreier, J.P., Körner, K., Ebert, N., Görner, A., Rubin, I., et al., 1998. Nitric oxide scavenging by hemoglobin or nitric oxide synthase inhibition by N-nitro-L-arginine induces cortical spreading ischemia when K⁺ is increased in the subarachnoid space. *J. Cerebr. Blood Flow Metabol.* 18 (9), 978–990. <https://doi.org/10.1097/00004647-199809000-00007>.

Dreier, J.P., Fabricius, M., Ayata, C., Sakowitz, O.W., Shuttleworth, C.W., et al., 2017. Recording, analysis, and interpretation of spreading depolarizations in neurointensive care: review and recommendations of the COSBID research group. *J. Cerebr. Blood Flow Metabol.* 37 (5), 1595–1625. <https://doi.org/10.1177/0271678X166654496>.

Dvoráček, S., Keresztes, A., Mollica, A., Stefanucci, A., Macedonio, G., et al., 2019. Preparation of bivalent agonists for targeting the mu opioid and cannabinoid receptors. *Eur. J. Med. Chem.* 178, 571–588. <https://doi.org/10.1016/j.ejmech.2019.05.037>.

Farkas, E., Luiten, P.G., Bari, F., 2007. Permanent, bilateral common carotid artery occlusion in the rat: a model for chronic cerebral hypoperfusion-related neurodegenerative diseases. *Brain Res. Rev.* 54 (1), 162–180. <https://doi.org/10.1016/j.brainresrev.2007.01.003>.

Farkas, E., Pratt, R., Sengpiel, F., Obrenovitch, T.P., 2008. Direct, live imaging of cortical spreading depression and anoxic depolarisation using a fluorescent, voltage-sensitive dye. *J. Cerebr. Blood Flow Metabol.* 28 (2), 251–262. <https://doi.org/10.1038/sj.jcbfm.9600569>.

Farkas, E., Obrenovitch, T.P., Institoris, Á., Bari, F., 2011. Effects of early aging and cerebral hypoperfusion on spreading depression in rats. *Neurobiol. Aging* 32 (9), 1707–1715. <https://doi.org/10.1016/j.neurobiolaging.2009.10.002>.

Fontanilla, D., Johannessen, M., Hajipour, A.R., Cozzi, N.V., Jackson, M.B., et al., 2009. The hallucinogen N,N-dimethyltryptamine (DMT) is an endogenous sigma-1 receptor regulator. *Science* 323 (5916), 934–937. <https://doi.org/10.1126/science.1166127>.

Frecska, E., Szabo, A., Winkelman, M.J., Luna, L.E., McKenna, D.J., 2013. A possibly sigma-1 receptor mediated role of dimethyltryptamine in tissue protection, regeneration, and immunity. *J. Neural. Transm.* 120 (9), 1295–1303. <https://doi.org/10.1007/s00702-013-1024-y>.

Ghanbari, R., El Mansari, M., Shahid, M., Blier, P., 2009. Electrophysiological characterization of the effects of asenapine at 5-HT(1A), 5-HT(2A), alpha(2)-adrenergic and D(2) receptors in the rat brain. *Eur. Neuropsychopharmacol.* 19 (3), 177–187. <https://doi.org/10.1016/j.euroneuro.2008.11.001>.

Gold, L., Back, T., Arnold, G., Dreier, J., Einhüpl, K.M., et al., 1998. Cortical spreading depression-associated hyperemia in rats: involvement of serotonin. *Brain Res.* 783 (2), 188–193. [https://doi.org/10.1016/s0006-8993\(97\)01341-3](https://doi.org/10.1016/s0006-8993(97)01341-3).

Guedes, R.C.A., Araújo, M.D.G.R., Verçosa, T.C., Bion, F.M., et al., 2017. Evidence of an inverse correlation between serotonergic activity and spreading depression propagation in the rat cortex. *Brain Res.* 1672, 29–34. <https://doi.org/10.1016/j.brainres.2017.07.011>.

Hall, A.A., Herrera, Y., Ajmo Jr., C.T., Cuevas, J., Pennypacker, K.R., 2009. Sigma receptors suppress multiple aspects of microglial activation. *Glia* 57 (7), 744–754. <https://doi.org/10.1002/glia.20802>.

Hartings, J.A., Shuttleworth, C.W., Kirov, S.A., Ayata, C., Hinzman, J.M., et al., 2017. The continuum of spreading depolarizations in acute cortical lesion development: examining Leão’s legacy. *J. Cerebr. Blood Flow Metabol.* 37 (5), 1571–1594. <https://doi.org/10.1177/0271678X16654495>.

Hayashi, T., 2015. Sigma-1 receptor: the novel intracellular target of neuropsychotropic drugs. *J. Pharmacol. Sci.* 127 (1), 2–5. <https://doi.org/10.1016/j.jphs.2014.07.001>.

Hayashi, T., 2019. The sigma-1 receptor in cellular stress signaling. *Front. Neurosci.* 13, 733. <https://doi.org/10.3389/fnins.2019.00733>.

Hayashi, T., Lewis, A., Hayashi, E., Betenbaugh, M.J., Su, T.P., 2011. Antigen retrieval to improve the immunocytochemistry detection of sigma-1 receptors and ER chaperones. *Histochem. Cell Biol.* 135 (6), 627–637. <https://doi.org/10.1007/s00418-011-0811-5>.

Hoffmann, U., Ayata, C., 2013. Neurovascular coupling during spreading depolarizations. *Acta Neurochir. Suppl.* 115, 161–165. https://doi.org/10.1007/978-3-7091-1192-5_31.

Ishima, T., Fujita, Y., Hashimoto, K., 2014. Interaction of new antidepressants with sigma-1 receptor chaperones and their potentiation of neurite outgrowth in PC12 cells. *Eur. J. Pharmacol.* 727, 167–173. <https://doi.org/10.1016/j.ejphar.2014.01.064>.

Jackman, K., Iadecola, C., 2015. Neurovascular regulation in the ischemic brain. *Antioxidants Redox Signal.* 22 (2), 149–160. <https://doi.org/10.1089/ars.2013.5669>, 2015.

Jahanbazi Jahan-Abad, A., Alizadeh, L., Sahab Negah, S., Barati, P., Khaleghi Ghadiri, M., et al., 2018. Apoptosis following cortical spreading depression in

- juvenile rats. *Mol. Neurobiol.* 55 (5), 4225–4239. <https://doi.org/10.1007/s12035-017-0642-z>.
- Jenner, P., Marsden, C.D., Thandi, C.M., 1978. Behavioural changes induced by N,N-dimethyltryptamine in rodents. *Br. J. Pharmacol.* 63 (2), 380P.
- Jia, J., Cheng, J., Wang, C., Zhen, X., 2018. Sigma-1 receptor-modulated neuroinflammation in neurological diseases. *Front. Cell. Neurosci.* 12, 314. <https://doi.org/10.3389/fncel.2018.00314>.
- Katnik, C., Garcia, A., Behensky, A.A., Yasny, I.E., Shuster, A.M., et al., 2016. Activation of σ_1 and σ_2 receptors by afobazole increases glial cell survival and prevents glial cell activation and nitrosative stress after ischemic stroke. *J. Neurochem.* 139 (3), 497–509. <https://doi.org/10.1111/jnc.13756>.
- Kilkenny, C., Browne, W., Cuthill, I.C., Emerson, M., Altman, D.G., 2010. Animal research: reporting in vivo experiments: the ARRIVE guidelines. *Br. J. Pharmacol.* 160, 1577–1579. <https://doi.org/10.1111/j.1476-5381.2010.00872.x>.
- Klass, A., Sánchez-Porras, R., Santos, E., 2018. Systematic review of the pharmacological agents that have been tested against spreading depolarizations. *J. Cerebr. Blood Flow Metabol.* 38 (7), 1149–1179. <https://doi.org/10.1177/0271678X18771440>.
- Klette, K.L., Lin, Y., Clapp, L.E., DeCoster, M.A., Moreton, J.E., et al., 1997. Neuroprotective sigma ligands attenuate NMDA and trans-ACPD-induced calcium signaling in rat primary neurons. *Brain Res.* 756 (1–2), 231–240. [https://doi.org/10.1016/s0006-8993\(97\)00142-x](https://doi.org/10.1016/s0006-8993(97)00142-x).
- Körmöczy, T., Í. Szabó, Farkas, E., Penke, B., Janáky, T., et al., 2020. Heart-cutting two-dimensional liquid chromatography coupled to quadrupole-orbitrap high resolution mass spectrometry for determination of N,N-dimethyltryptamine in rat plasma and brain; method development and application. *J. Pharmaceut. Biomed. Anal.* 191, 30. <https://doi.org/10.1016/j.jpba.2020.113615>, 2020.
- Kucharz, K., Lauritzen, M., 2018. CaMKII-dependent endoplasmic reticulum fission by whisker stimulation and during cortical spreading depolarization. *Brain* 141 (4), 1049–1062. <https://doi.org/10.1093/brain/awy036>.
- Leao, A.A.P., 1944. Spreading depression of activity in the cerebral cortex. *J. Neurophysiol. (Bethesda)* 7, 359–390. <https://doi.org/10.1152/jn.1944.7.6.359>.
- Lukaszewicz, A.C., Sampaio, N., Guégan, C., Benchoua, A., Couriaud, C., et al., 2002. High sensitivity of protoplasmic cortical astroglia to focal ischemia. *J. Cerebr. Blood Flow Metabol.* 22 (3), 289–298. <https://doi.org/10.1097/00004647-200203000-00006>.
- Luna, L.E., 2011. Indigenous and mestizo use of ayahuasca: an overview. In: Dos Santos, R.G. (Ed.), *The Ethnopharmacology of Ayahuasca*. Transworld Research Network, Kerala, pp. 1–21.
- Mandel, L.R., Prasad, R., Lopez-Ramos, B., Walker, R.W., 1977. The biosynthesis of dimethyltryptamine in vivo. *Res. Commun. Chem. Pathol. Pharmacol.* 16 (1), 47–58.
- Maurice, T., Su, T.P., Parish, D.W., Privat, A., 1995. Prevention of nimodipine-induced impairment of learning by the selective sigma ligand PRE-084. *J. Neural Transm. Gen. Sect.* 102 (1), 1–18. <https://doi.org/10.1007/BF01276561>.
- Mavlyutov, T.A., Epstein, M.L., Liu, P., Verby, Y.I., Ziskind-Conhaim, L., Ruoho, A.E., 2012. Development of the sigma-1 receptor in C-terminals of motoneurons and colocalization with the N,N-dimethyltryptamine forming enzyme, indole-N-methyl transferase. *Neuroscience* 206, 60–68. <https://doi.org/10.1016/j.neuroscience.2011.12.040>.
- Menyhárt, Á., Zólei-Szénási, D., Puskás, T., Makra, P., Orsolya, M.T., Szepes, B.É., Tóth, R., Ivánkovits-Kiss, O., Obrenovitch, T.P., Bari, F., Farkas, E., 2017. Spreading depolarization remarkably exacerbates ischemia-induced tissue acidosis in the young and aged rat brain. *Sci. Rep.* 7 (1), 1154. <https://doi.org/10.1038/s41598-017-01284-4>.
- Mies, G., 1998. Neuroprotective effect of sumatriptan, a 5-HT_{1D} receptor agonist, in focal cerebral ischemia of rat brain. *J. Stroke Cerebrovasc. Dis.* 7 (4), 242–249. [https://doi.org/10.1016/s1052-3057\(98\)80033-5](https://doi.org/10.1016/s1052-3057(98)80033-5).
- Nardai, S., László, M., Szabó, A., Alpár, A., Hanics, J., et al., 2020. N,N-dimethyltryptamine reduces infarct size and improves functional recovery following transient focal brain ischemia in rats. *Exp. Neurol.* 327, 113245. <https://doi.org/10.1016/j.expneurol.2020.113245>.
- Narita, N., Hashimoto, K., Tomitaka, S., Minabe, Y., 1996. Interactions of selective serotonin reuptake inhibitors with subtypes of sigma receptors in rat brain. *Eur. J. Pharmacol.* 307, 117–119. [https://doi.org/10.1016/0014-2999\(96\)00254-3](https://doi.org/10.1016/0014-2999(96)00254-3).
- Omi, T., Tanimukai, H., Kanayama, D., Sakagami, Y., Tagami, S., et al., 2014. Fluvoxamine alleviates ER stress via induction of Sigma-1 receptor. *Cell Death Dis.* 5, e1332 <https://doi.org/10.1038/cddis.2014.301>.
- Penke, B., Fulop, L., Szucs, M., Frecska, E., 2018. The role of sigma-1 receptor, an intracellular chaperone in neurodegenerative diseases. *Curr. Neuropharmacol.* 16 (1), 97–116. <https://doi.org/10.2174/1570159X15666170529104323>.
- Ray, T.S., 2010. Psychedelics and the human receptorome. *PLoS One* 5 (2), 1–17. <https://doi.org/10.1371/journal.pone.0009019>.
- Rehm, M., Dussmann, H., Janicke, R.U., Tavare, J.M., Kogel, D., et al., 2002. Single-cell fluorescence resonance energy transfer analysis demonstrates that caspase activation during apoptosis is a rapid process. Role of caspase-3. *J. Biol. Chem.* 277 (27), 24506–24514. <https://doi.org/10.1074/jbc.M110789200>.
- Reinhart, K.M., Shuttleworth, C.W., 2018. Ketamine reduces deleterious consequences of spreading depolarizations. *Exp. Neurol.* 305, 121–128. <https://doi.org/10.1016/j.expneurol.2018.04.007>.
- Richter, F., Ebersberger, A., Schaible, H.G., 2002. Blockade of voltage-gated calcium channels in rat inhibits repetitive cortical spreading depression. *Neurosci. Lett.* 334 (2), 123–126. [https://doi.org/10.1016/s0304-3940\(02\)01120-5](https://doi.org/10.1016/s0304-3940(02)01120-5).
- Rossi, D.J., Brady, J.D., Mohr, C., 2007. Astrocyte metabolism and signaling during brain ischemia. *Nat. Neurosci.* 10 (11), 1377–1386. <https://doi.org/10.1038/nn2004>.
- Ruscher, K., Inácio, A.R., Valind, K., Rowshan Ravan, A., Kuric, E., et al., 2012. Effects of the sigma-1 receptor agonist 1-(3,4-dimethoxyphenethyl)-4-(3-phenylpropyl)-piperazine dihydro-chloride on inflammation after stroke. *PLoS One* 7 (9), e45118. <https://doi.org/10.1371/journal.pone.0045118>, 2012.
- Sato, S., Kawamata, T., Kobayashi, T., Okada, Y., 2014. Antidepressant fluvoxamine reduces cerebral infarct volume and ameliorates sensorimotor dysfunction in experimental stroke. *Neuroreport* 25 (10), 731–736. <https://doi.org/10.1097/WNR.0000000000000162>.
- Schneider, C.A., Rasband, W.S., Eliceiri, K.W., 2012. NIH image to ImageJ: 25 Years of image analysis. *Nat. Methods* 9 (7), 671–675. <https://doi.org/10.1038/nmeth.2089>, 2012.
- Shahid, M., Walker, G.B., Zorn, S.H., Wong, E.H., 2009. Asenapine: a novel psychopharmacologic agent with a unique human receptor signature. *J. Psychopharmacol.* 23 (1), 65–73. <https://doi.org/10.1177/0269881107082944>.
- Siesjö, B.K., Bengtsson, F., 1989. Calcium fluxes, calcium antagonists, and calcium-related pathology in brain ischemia, hypoglycemia, and spreading depression: a unifying hypothesis. *J. Cerebr. Blood Flow Metabol.* 9 (2), 127–140. <https://doi.org/10.1038/jcbfm.1989.20>.
- Sitaram, B.R., Lockett, L., Talomsin, R., Blackman, G.L., McLeod, W.R., 1987. In vivo metabolism of 5-methoxy-N,N-dimethyltryptamine and N,N-dimethyltryptamine in the rat. *Biochem. Pharmacol.* 36 (9), 1509–1512. [https://doi.org/10.1016/0006-2952\(87\)90118-3](https://doi.org/10.1016/0006-2952(87)90118-3), 1987.
- Somjen, G.G., 2001. Mechanisms of spreading depression and hypoxic spreading depression-like depolarization. *Physiol. Rev.* 81 (3), 1065–1096. <https://doi.org/10.1152/physrev.2001.81.3.1065>.
- Stockwell, B.R., Friedmann Angeli, J.P., Bayir, H., Bush, A.I., Conrad, M., et al., 2017. Ferroptosis: a regulated cell death nexus linking metabolism, redox Biology, and disease. *Cell* 171 (2), 273–285. <https://doi.org/10.1016/j.cell.2017.09.021>.
- Strassman, R.J., 2001. DMT: The Spirit Molecule. A Doctor's Revolutionary Research into the Biology of Near-Death and Mystical Experiences. Park Street Press, Rochester, Vermont, USA.
- Strassman, R.J., Qualls, C.R., 1994. Dose-response study of N,N-dimethyltryptamine in humans. I. Neuroendocrine, autonomic, and cardiovascular effects. *Arch. Gen. Psychiatr.* 51 (2), 85–97. <https://doi.org/10.1001/archpsyc.1994.03950020009001>.
- Szabó, A., Frecska, E., 2016. Dimethyltryptamine (DMT): a biochemical Swiss Army knife in neuroinflammation and neuroprotection? *Neural Regen Res* 11 (3), 396–397. <https://doi.org/10.4103/1673-5374.179041>.
- Szabó, A., Kovacs, A., Frecska, E., Rajnavolgyi, E., 2014. Psychedelic N,N-dimethyltryptamine and 5-methoxy-N,N-dimethyltryptamine modulate innate and adaptive inflammatory responses through the sigma-1 receptor of human monocyte-derived dendritic cells. *PLoS One* 9 (8), e106533. <https://doi.org/10.1371/journal.pone.0106533>.
- Szabó, A., Kovacs, A., Riba, J., Djurovic, S., Rajnavolgyi, E., et al., 2016. The endogenous hallucinogen and trace amine N,N-dimethyltryptamine (DMT) displays potent protective effects against hypoxia via sigma-1 receptor activation in human primary iPSC-derived cortical neurons and microglia-like immune cells. *Front. Neurosci.* 10, 423. <https://doi.org/10.3389/fnins.2016.00423>.
- Szabó, I., M Tóth, O., Török, Z., Varga, D.P., Menyhárt, Á., et al., 2019. The impact of dihydropyridine derivatives on the cerebral blood flow response to somatosensory stimulation and spreading depolarization. *Br. J. Pharmacol.* 176 (9), 1222–1234. <https://doi.org/10.1111/bph.14611>.
- Sztybel, K., Tymianski, M., 2010. Calcium, ischemia and excitotoxicity. *Cell Calcium* 47 (2), 122–129. <https://doi.org/10.1016/j.ceca.2010.01.003>.
- Teschendorf, P., Padosch, S.A., Spöhr, F., Albertsmeier, M., Schneider, A., et al., 2008. Time course of caspase activation in selectively vulnerable brain areas following global cerebral ischemia due to cardiac arrest in rats. *Neurosci. Lett.* 448 (2), 194–199. <https://doi.org/10.1016/j.neulet.2008.10.030>.
- Tóth O, M., Á. Menyhárt, Varga, V.É., Hantosi, D., Ivánkovits-Kiss, O., et al., 2020. Chitosan nanoparticles release nimodipine in response to tissue acidosis to attenuate spreading depolarization evoked during forebrain ischemia. *Neuropharmacology* 162, 107850. <https://doi.org/10.1016/j.neuropharm.2019.107850>.
- Varga, D.P., Puskás, T., Á. Menyhárt, Hertelendy, P., Zólei-Szénási, D., et al., 2016. Contribution of prostanoid signaling to the evolution of spreading depolarization and the associated cerebral blood flow response. *Sci. Rep.* 6, 31402. <https://doi.org/10.1038/srep31402>.
- Varga, D.P., Í. Szabó, Varga, V.É., Á. Menyhárt, Tóth O, M., et al., 2020. The antagonism of prostaglandin FP receptors inhibits the evolution of spreading depolarization in an experimental model of global forebrain ischemia. *Neurobiol. Dis.* 137, 104780. <https://doi.org/10.1016/j.nbd.2020.104780>, 2020.
- von Bornstädt, D., Houben, T., Seidel, J.L., Zheng, Y., Dilekoz, E., et al., 2015. Supply-demand mismatch transients in susceptible peri-infarct hot zones explain the origins of spreading injury depolarizations. *Neuron* 85 (5), 1117–1131. <https://doi.org/10.1016/j.neuron.2015.02.007>.
- Yanai, K., Ido, T., Ishiwata, K., Hatazawa, J., Takahashi, T., et al., 1986. In vivo kinetics and displacement study of a carbon-11-labeled hallucinogen, N,N-[11C]dimethyltryptamine. *Eur. J. Nucl. Med.* 12 (3), 141–146. <https://doi.org/10.1007/BF00276707>.
- Zhang, H., Cuevas, J., 2002. Sigma receptors inhibit high-voltage-activated calcium channels in rat sympathetic and parasympathetic neurons. *J. Neurophysiol.* 87 (6), 2867–2879. <https://doi.org/10.1152/jn.2002.87.6.2867>.
- Zhang, X., Wu, F., Jiao, Y., Tang, T., Yang, L., et al., 2017. An increase of sigma-1 receptor in the penumbra neuron after acute ischemic stroke. *J. Stroke Cerebrovasc. Dis.* 26 (9), 1981–1987. <https://doi.org/10.1016/j.jstrokecerebrovasdis.2017.06.013>.
- Zhao, X., Zhu, L., Liu, D., Chi, T., Ji, X., et al., 2019. Sigma-1 receptor protects against endoplasmic reticulum stress-mediated apoptosis in mice with cerebral ischemia/reperfusion injury. *Apoptosis* 24 (1–2), 157–167. <https://doi.org/10.1007/s10495-018-1495-2>.